Surface currents in operational oceanography: Key applications, mechanisms, and methods

Johannes Röhrs, Graig Sutherland, Gus Jeans, Michael Bedington, Ann Kristin Sperrevik, Knut-Frode Dagestad, Yvonne Gusdal, Cecilie Mauritzen, Andrew Dale & Joseph H. LaCasce

Published online: 23 Mar 2021.

Submit your article to this journal ⤤

Article views: 1151

View related articles ⤤

View Crossmark data ⤤

Taylor & Francis
Taylor & Francis Group

∂ OPEN ACCESS | Check for updates

Surface currents in operational oceanography: Key applications, mechanisms, and methods

Johannes Röhrs [a], Graig Sutherland [b], Gus Jeans[c], Michael Bedington [d], Ann Kristin Sperrevik [a], Knut-Frode Dagestad [a], Yvonne Gusdal[a], Cecilie Mauritzen [a], Andrew Dale[e] and Joseph H. LaCasce [f]

aDivision for Ocean and Ice, Norwegian Meteorological Institute, Oslo, Norway; bMeteorological Research Division, Environment and Climate Change Canada, Dorval, QC, Canada; cOceanalysis Ltd., Wallingford, UK; dPlymouth Marine Laboratory, Plymouth, UK; eScottish Association for Marine Science, Scottish Marine Institute, Oban, UK; fDepartment of Geosciences, University of Oslo, Oslo, Norway

ABSTRACT

This paper reviews physical mechanisms, observation techniques and modelling approaches dealing with surface currents on short time scales (hours to days) relevant for operational oceanography. Key motivations for this article include fundamental difficulties in reliable measurements and the persistent lack of a widely held consensus on the definition of surface currents. These problems are augmented by the fact that various methods to observe and model ocean currents yield very different representations of a surface current. We distinguish between four applicable definitions for surface currents; (i) the interfacial surface current, (ii) the direct wind-driven surface current, (iii) the surface boundary layer current, and (iv) an effective drift current. Finally, we discuss challenges in synthesising various data sources of surface currents - i.e. observational and modelling – and take a view on the predictability of surface currents concluding with arguments that parts of the surface circulation exhibit predictability useful in an operational context.

1. Introduction

Surface currents are a central subject in operational oceanography with rapidly growing observing and forecasting capabilities. We are entering an era where observations provide a sufficient level of detail, and numerical models the predictive skill, for applications to use surface current information to aid marine safety, value creation and environmental monitoring. Observation techniques now provide real-time surface current fields at the scale of kilometres (Isern-Fontanet et al. 2017), and high-resolution ocean models are on the verge of having predictive skill on short time scales (Jacobs et al. 2014b; Sandery and Sakov 2017; Christensen et al. 2018). In this context, we consider short time scales, i.e. time scales characterised by the inertial period (hours to a few days).

This work is motivated by challenges in obtaining and understanding observations and model data of ocean currents near the surface. Differing designs of Lagrangian drifters, as illustrated in Figure 1, show very different behaviour (Poulain et al. 2009; Morey et al. 2018), and Eulerian current meter poorly resolve the surface. A challenge in modelling is to resolve vertical shear in the upper few centimetres to decimetres that has a substantial bearing on some drift applications (Figure 1). Consistent synthesis between *in situ* measurements, remote sensing and modelling is needed in the analysis of surface currents because each method provides a unique representation of surface current dynamics, as illustrated in Figure 2. Yet there is no consensus on which depth and time scale the term 'surface current' refers to (Laxague et al. 2018).

Applications that need information and predictions of surface currents encompass industrial activities, governmental services, and environmental studies. An overview is given in Figure 3. All of the listed activities are affected by ocean currents at or near the surface, however, the associated depth range and time scope differs.

For most of these applications, usage of ocean currents from operational forecasting has long been hampered by the chaotic nature of oceanic flow and its variability on scales not covered by observation networks. Ocean currents are comprised of numerous

CONTACT Johannes Röhrs ✉ johannes.rohrs@met.no ☐ Division for Ocean and Ice, Norwegian Meteorological Institute, Henrik Mohns Plass, 1, Oslo, Norway
This article has been republished with minor changes. These changes do not impact the academic content of the article.
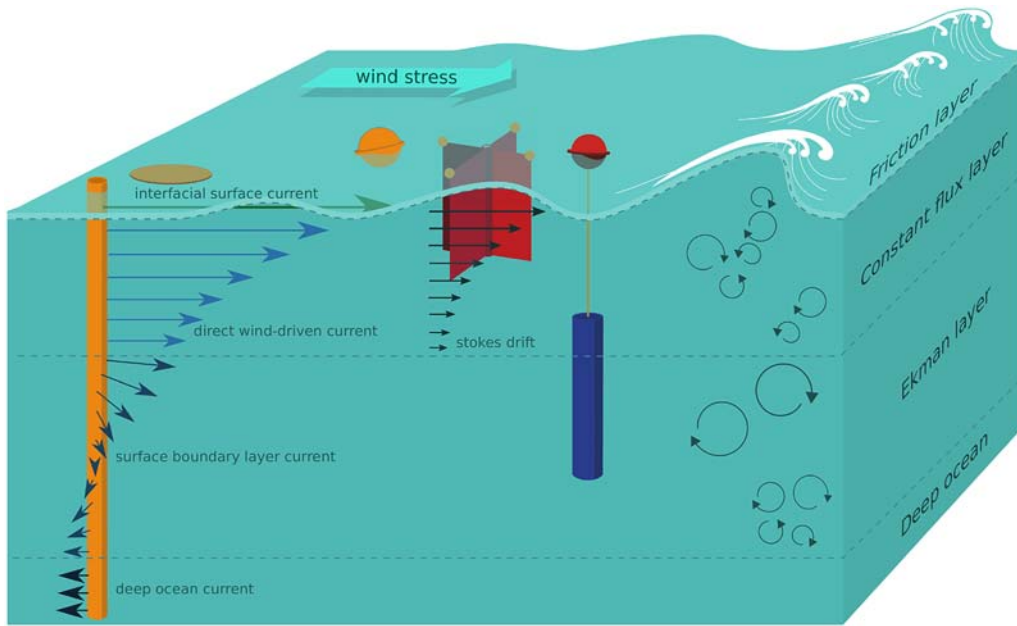
Figure 1. Schematic view of surface current regimes and types of surface drifters. In this view, the ocean surface boundary layer is divided into the friction layer, the constant flux layer, and the Ekman layer. The entire boundary layer is characterised by elevated turbulent mixing, with largest and most efficient mixing in the interior and lower mixing near the surface and at the base of the mixed layer. Surface currents are characterised by strong wind-driven shear of velocity magnitude in the friction layer and the constant flux layer, and a strong shear in direction throughout the Ekman layer. The direction of the deep ocean current is arbitrary in this illustration and is in practice not related to the wind direction. Surface drifters, from left to right: Bamboo plate, iSphere drifter, drogued CODE-drifter, drogued SVP-drifter.

phenomena, from large-scale geostrophic currents, to eddies and fronts at intermediate scales (Chelton et al. 2007), and Langmuir circulation cells that approach the scale of oceanic turbulence (McWilliams et al. 2012). Other components of ocean currents are better distinguished by their temporal variation, for example, tides and wind-driven near inertial waves (Alford and Gregg 2001).

A frequent use of operational ocean circulation models is the prediction of drift trajectories (Griffa et al. 2007). For oceanic drift at or near the ocean surface, it is critical to use the current at the target depth for the application considered, as drift in the uppermost part of the ocean differs greatly with depth. However, ocean models often do not resolve the near-surface gradients of wind-induced shear (e.g. Chassignet and Verron 2006; Dagestad and Röhrs 2019), or they lack coupling mechanisms for air-wave-sea interactions to describe strongly forced drift in severe weather events.
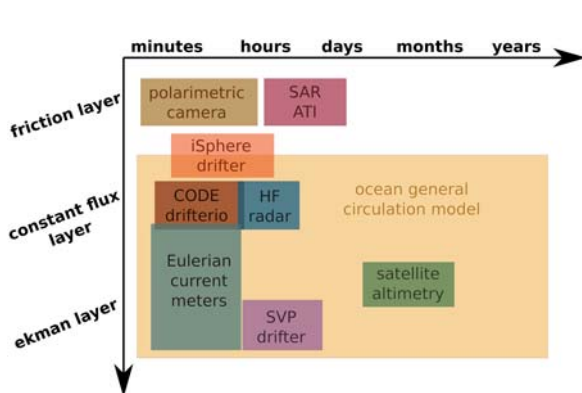
Figure 2. Methods that provide information on surface currents, organised by the depth and time scales that are resolved by each method. In this paper, we focus on methods that cover short time scales of hours to a few days.
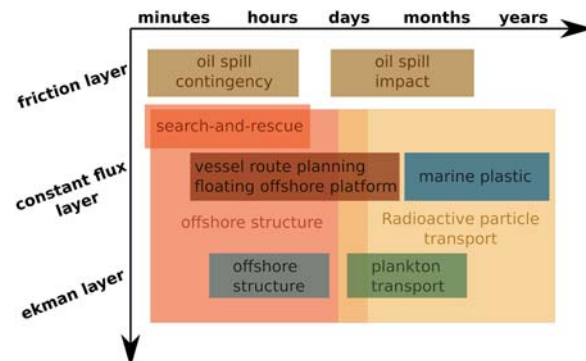
Figure 3. Applications that utilise surface current data, organised by the involved depth and time scales that are relevant for each application. Surface current information in operational oceanography mostly require to describe short time scales of hours to days.

When referring to surface currents, it should always be clear which part of the ocean circulation is meant. We suggest a classification for surface currents in this review, based on a review of surface current mechanisms and applications that require current information. A clearer definition of surface currents was also highlighted as a priority by the surface current working group arising from the first meeting of the Australian Forum for Operational Oceanography in 2015. They recommend that users and suppliers of ocean information be very clear about what depth below the surface and averaging timescales are applicable.

Section 2 describes the most common applications, and what type of information they require. We provide an overview of the physical mechanisms that govern surface currents in Section 3. Section 4 reviews observation techniques and to which application each of them is best suited. Surface current products from models are discussed in Section 5, with a particular section considering particle tracking models. The discussion (Section 6) includes a suggested terminology for surface currents, and a view on the variability and predictability of surface currents.

Other reviews that treat surface currents include Isern-Fontanet et al. (2017), which focuses on remote sensing and data assimilation, Shutler et al. (2016) and Le Traon et al. (2015), who treat satellite observations of the ocean surface, and Lumpkin et al. (2017), covering the use of Lagrangian drifters to study surface currents. Possibilities for short-term drift predictions are explored in Christensen et al. (2018), and LaCasce (2008) and van Sebille et al. (2018) consider a range of analysis techniques for Lagrangian data relevant for surface circulation.

2. Applications for surface current data

The vast majority of human activity in the oceans occurs at the surface and is affected by surface currents, yielding a wide range of users (Table 1). The table includes applicable depth range and time scales, following the improved clarity recommend by the Australian Forum for Operational Oceanography (2015).

The Global Ocean Observing System (GOOS) Ocean Observations Panel for Climate (OOPC, 2017) has defined surface currents as one of the key physical Essential Ocean Variables (EOV), and surface currents are a key meteorological and oceanographic parameter for the offshore energy industries. Reliable quantification is a primary requirement in all stages of a project life cycle, which are similar for hydrocarbon and offshore renewables and include asset appraisal, survey, engineering design, installation, operations, maintenance and decommissioning. In each stage, user requirements include long-term hindcasting of past conditions, accurate determination of present conditions and realistic forecasts (Cooper et al. 2016). The quantification of currents has a critical role in assessments for marine renewable power, e.g. tidal energy (McCann and Bell 2014; Ferreira et al. 2016).

Trajectory modelling is a common application of operational ocean model data. This includes drift modelling for Search-and-Rescue assistance (Breivik et al. 2013), prediction of floating icebergs (e.g. Keghouche et al. 2009), and the drift of marine debris. Prominent examples are the tracing of debris following the tsunami wave near Fukushima in 2011 (Matthews et al. 2017), and debris trajectories of the lost flight MH370 disappearing over the Indian Ocean in 2014 (Trinanes et al. 2016).

Oil spill preparedness is needed for oil exploitation and shipping in general, and surface currents are the most important variable for an oil spill model for short time scales. As the majority of oil is found as a slick at the surface, surface current information that represents the upper few centimetres, in addition to wind and wave data, is required for modelling (De Dominicis et al. 2016; Jones et al. 2016). As parts of an oil spill also become submerged, oil spill models require the full current profile for the mixed layer

Table 1. Applications and user requirements of surface current information.

Application	Depth range	Time scale
Seismic survey	Streamer depth	Hours to days
Fixed offshore platform	Full profile	Hours to years
Floating offshore platform	Full profile with focus on platform draft	Hours to years
Oil spill at surface	Surface film and upper mixed layer	Hours to months
Oil spill, deep blowout	Full profile	Days to months
Search and Rescue	Average over effective object draft	Hours to days
Marine debris	Depth of debris parts	Days to years
Vessel route planning	Vessel draft	Hours
Ichthyoplankton transport	Full profile with focus on mixed layer	Days to months
Harmful algae	Full profile with focus on mixed layer	Days to weeks
Marine plastic	Full profile with focus on mixed layer	Months to years
Radioactive particles	Full profile	Days to years
Aquaculture	Mixed layer	Days to months

with increased level of detail near the surface. Search and Rescue and oil spill modelling systems are widely applied as commercial products (e.g. SARMAP by RPS group, OSCAR by Sintef Ocean).

Plankton transport and ecosystem models also require the full vertical profile of surface currents, with an increased level of detail in the mixed layer as the majority of primary production occur in the upper part of the ocean. Examples of plankton modelling in operational oceanography include the prediction of harmful algal blooms (Aleynik et al. 2016) and ichthyoplankton transport needed for the assessment of fish stock recruitment (Vikebø et al. 2011). In addition to plankton transport, the transport of plastic in the ocean is a topic of increasing interest to the oceanography community (Law 2017). As plastics can readily be transported within the water column Kukulka et al. (2012), the vertical profile of surface currents can affect the pathways and distribution of plastics in the ocean (Wichmann et al. 2019).

3. Physical mechanisms

In this section, the dominant mechanisms associated with surface currents will be discussed. The focus will be on mechanisms associated with the surface ocean on short time scales – i.e. hours to few days – such as wind forcing, ocean turbulence, and surface gravity waves. Other important oceanographic elements include geostrophically balanced flows, tides, topographical steering, and mesoscale eddies; but while relevant to the ocean surface, they are not limited to it and are thus given only minor attention in this article.

3.1. Wind-induced currents

The winds are a major driving element for near-surface ocean currents. It is convenient to break wind-driven flows into those for which the wind stress plays a direct dynamical role, and those less directly wind-driven, whether by the recent wind history (near-inertial oscillations), by wind-driven waves (Stokes drift), or by the wind-forced redistribution of water leading to surface slopes and geostrophic flow (basin-scale gyres and equatorial current systems). The mesoscale and smaller variability that often dominates oceanic kinetic energy results from instability of the larger scale flows, which in turn are driven by wind and thermohaline forcing (e.g. Vallis 2017). The directly and indirectly wind-driven contributions are considered separately hereafter as they have quite different timescales and manifestations in observations.

Steady-state Ekman current

A classical view of the wind-driven current are steady-state solutions of the ocean surface boundary layer (OSBL). In Ekman's seminal solution, there is a balance between the vertical shear stress and the Coriolis force in the boundary layer, with wind stress providing the upper boundary condition (Ekman 1905). In Ekman's solution, the (ageostrophic) surface current is 45° to the right of the wind in the northern hemisphere, and the velocities decay with depth, turning to the right in an 'Ekman spiral' (indicated in the lower portion of Figure 1). Allowing for more realistic vertical mixing which varies with depth and stratification, alters the deflection and the decay, but not the qualitative picture (Lentz 2001).

The flow is rarely in an actual steady-state as there exists significant wind variance at sub-inertial periods. Therefore, Ekman's solution only prevails in observations when time- or sample-averaging is applied (Lenn and Chereskin 2009). Through time-averaging, Gonella (1972) identified an Ekman layer in observations from moored current meter, and Niiler and Paduan (1995) in drifter experiments. Ralph and Niiler (1999) estimated from surface drifters that 40% of the currents at 15 m depth in a weakly stratified mixed layer are explained by steady-state Ekman dynamics. Rio and Hernandez (2003) exploit the low-frequency relationship between winds and surface currents using an empirical model for the Ekman layer. The authors found that the steady-state assumption could be applied for periods of 20 days and longer. Combining such Ekman currents with satellite-derived geostrophic currents yields surface current estimations (Rio et al. 2014) that are useful for trajectory modelling in hindsight and nowcasting (Dagestad and Röhrs 2019).

Time-dependent response

Detailed descriptions of surface currents on the scale of hours to days must account for rapid changes in wind and wave conditions. V. Ekman included a time-dependent solution for the evolving Ekman spiral in his original work (Ekman 1905), and (Røed 1977) examined the adjustment to the steady-state solution. A general frequency dependent description of the ocean surface response to wind forcing is given by Elipot and Gille (2009a), who derive a transfer function in spectral space for the air–sea momentum flux. Such spectral transfer functions may be applied to analyse arbitrary wind forcing allowing for investigations beyond analytically prescribed wind patterns, e.g. observational wind records (e.g. Gonella 1972). At low frequencies – for time scales much longer than the inertial period –

surface currents approach the steady state Ekman balance. The maximum response to wind forcing occurs if the wind changes in strength or direction with the inertial frequency, generating near-inertial oscillations (NIOs) (D'Asaro 1985; Crawford and Large 1996). NIOs are horizontally isotropic currents that turn clockwise in the northern hemisphere at a near-inertial frequency, while their amplitude decays over several days.

Any adaptation of surface currents to variations in wind or OSBL thickness takes the form of NIOs to some degree (Madsen 1977; Christensen et al. 2018). In the presence of stratification, NIOs have a vertical component and are better referred to as near-inertial waves. These can also be forced by buoyancy fluxes in addition to wind forcing. Shallow and stable stratification, under which the upper layer can slide with little turbulent drag over deeper layers, permit stronger NIOs at the surface and reduce downward propagation (Shrira and Forget 2015).

NIOs are an energetic feature of the open ocean and often dominate the surface current signal in drifter observations (Poulain et al. 1992) and moored current records after wind events (e.g. D'Asaro et al. 1995). Their signature is also visible in time series of waves that are refracted by the inertial currents (Gemmrich and Garrett 2012). D'Asaro et al. (1995) presented a case study of the OSBL response to a storm over the North Pacific, generating homogeneous NIOs of 5 cm/s magnitude that lasted for 21 days.

Turbulence and vertical regimes in the OSBL

Turbulence is the mechanism that defines the oceanic surface boundary layer (OSBL), controlling how surface currents vary with depth (e.g. Madsen 1977; Lewis and Belcher 2004). In numerical models, turbulence is represented using an eddy viscosity for the vertical exchange of momentum. Ekman's solution for the variation of currents with depth assumes a constant eddy viscosity, while more realistic models for the OSBL require a depth-dependent viscosity.

With respect to major dynamic balances, the OSBL can be divided into three parts: the friction layer, a constant flux layer, and the Ekman layer. This distinction originates from atmospheric boundary layer theory (Stull 1988) and is similarly applicable to the OSBL (Craig and Banner 1994). We use these turbulent regimes to identify surface currents of each layer in Table 2.

The Ekman layer is the lower and major part of the OSBL, where the local force balance is predominantly between vertical mixing of momentum and the Coriolis force. The eddy viscosity reaches a maximum in the Ekman layer, such that Ekman's model applies approximately, i.e. a change of current direction and magnitude with depth provides the transition from the wind-induced surface current to the geostrophically balanced flow below the OSBL.

The 'constant flux layer' lies between the surface and Ekman layers. Here the vertical flux of horizontal momentum flux is constant with depth. The eddy viscosity increases linearly with depth, constituting the so-called *law of the wall*, meaning that turbulent eddies become larger away from the surface that confines their size. This regime implies immediate adjustment to equilibrium flow and a logarithmic velocity profile for neutral stratification (O'Brien 1970), associated with a smaller surface deflection angle of about $10°$ (Madsen 1977) and a 'flatter' spiral compared to the Ekman's solution.

The friction layer is a very thin part at the surface where viscous forces and disruption of the air–sea interface through wave breaking affect the velocity and diffusivity profiles. This leads to high downwind velocities with intense vertical shear in the upper centimetres (Wu 1984; Laxague et al. 2018; Morey et al. 2018). Under strong winds, breaking waves increase turbulence at the surface (Agrawal et al. 1992), such that an increase in the near-surface eddy viscosity will cause the surface deflection angle between wind and the current to increase relative to the law of the wall (Craig and Banner 1994).

Turbulence ultimately determines how the transition of momentum from the ocean surface to deeper layers occurs. Low turbulence, i.e. inefficient vertical mixing of momentum, means that momentum is confined near the surface – resulting in larger surface velocities and strong vertical shear. This is accompanied by a small surface deflection angle to the wind with strong veering towards deeper layers. With strong turbulence, momentum from the wind is more evenly distributed throughout the OSBL, resulting in weaker vertical gradients.

Sophisticated models for turbulence and current shear have been developed to describe the constant

Table 2. Terminology for surface currents.

	Dynamical regime	Depth scale	Time scale
Interfacial surface current	Friction layer	$\mathcal{O}(\text{mm})$	Seconds
Direct wind-driven current	Constant-flux layer	$\mathcal{O}(1–10\text{ m})$	Hours
Surface boundary layer current	Ekman layer	$\mathcal{O}(10–100\text{ m})$	Days
Effective drift current		Objects extend in water column	

flux layer and the Ekman layer (e.g. Large et al. 1994; Lewis and Belcher 2004; Umlauf and Burchard 2005). In situ observations indicate additional shear in the upper centimetre with strong downwind ocean velocities (Wu 1984; Laxague et al. 2018). Oil-slicks, marine debris, and plastics are shown to experience such a downwind motion which is not due to direct wind drag but strongly sheared currents in the upper centimetres (Jones et al. 2016).

Near-surface stratification

While wind and waves are the primary source of turbulence in the ocean surface boundary layer, stratification can either dampen or increase turbulence, affecting in turn the vertical shear (Stull 1988). With stable stratification near the surface, the shallow less-dense layer can slide downwind with low resistance from the layer below. This phenomenon, coined *slippery water* (Houghton and Woods 1969), can be important for marine applications, e.g. during sailing. In fact, it was used successfully by sailors during the 1968 Summer Olympics in Acapulco, Mexico. To quote David Houghton, who was the meteorological advisor to the British crews,

> For the first two weeks, the surface … behaved just like the slippery layer which had been postulated …. The surface water moved almost directly downwind at speeds of up to about 2 knots, depending on how long the wind had been blowing from that particular direction. When the wind dropped to a calm the water continued in the same direction with little change in speed and it took a wind from the opposite direction from 24 to 36 h to stop the water and get it moving the other way (Houghton 1969).

It has been shown that it is convenient to model the slippery layer as a slab of thickness h with a uniform velocity where the acceleration of the slab is given by Pollard and Millard (1970)

$$\frac{\partial u}{\partial t} - fv = \frac{\tau}{\rho h} - ru \qquad (1)$$

$$\frac{\partial v}{\partial t} + fu = -rv, \qquad (2)$$

where u is the along-wind velocity, v is the cross-wind velocity, τ is the wind stress (usually parameterised as $\tau = \rho_a C_D U_{10}^2$, where ρ_a is the air density C_D is the drag coefficient and U_{10} is the wind speed referenced to 10 m) and r is a linearised friction coefficient associated with the temporal decay scale of the slab layer, typically of the order of $1/r = 4$ days (D'Asaro 1985). What is clear from Equations (1) and (2) is that the acceleration of the slab is initially in the direction of the wind

and rotates due to the Coriolis force. For small values of t, i.e. $rt \ll 1$ and $ft \ll 1$, the time evolution of the slab, assuming h, τ and ρ are constant, is

$$u(t) - u(0) = \frac{\tau t}{\rho h}. \qquad (3)$$

Equation (3) states that the surface current increases linearly with time and is inversely proportional to the thickness h. For example, a wind speed of about 5 m/s and a slab layer thickness of 1 m would give an increase in the along-wind surface current of about 0.25 m/s after 2 h. However, caution is required when using Equations (1) and (2) as the model assumes that the buoyancy jump at the base of the slab is large enough to limit vertical exchange. Otherwise, the slippery layer will quickly erode either from turbulent mixing or shear instabilities generated at its lower interface (Kudryavtsev and Soloviev 1990; Sutherland et al. 2016). Freshwater fluxes from rivers, rainfall, or very strong diurnal heating can cause such stratification.

A common occurrence of slippery layers is the "diurnal jet", which can emerge during relatively low wind and high solar insolation (Price et al. 1986; Kudryavtsev and Soloviev 1990; Sutherland et al. 2016). The diurnal jet is associated with the diurnal variability in SST and is observed at all latitudes, but most often in tropical and sub-tropical regions (Gentemann 2003; Stuart-Menteth 2003; Kawai and Wada 2007).

Under favourable wind conditions, the diurnal jet begins as soon as sufficient stratification is created due to the shortwave insolation. The diurnal jet is initially aligned with the wind and increases linearly with time, as given by (3) and turns subject to the Coriolis force. The diurnal jet is often on the order of 10 cm/s (Price et al. 1986; Sutherland et al. 2016), which can be comparable to the night-time near-surface current in these regions.

3.2. Wave-induced surface currents

This section describes how surface gravity waves affect surface currents, either through wave-current interaction or direct contribution to drift velocities. Waves also affect turbulence below the surface (McWilliams et al. 2012).

The Stokes drift from surface gravity waves

Surface gravity waves cause particle transport in the direction of wave propagation, which is referred to as Stokes drift (Stokes 1847; van den Bremer and Breivik 2018). Stokes drift is not included in current observations at fixed locations nor in ocean circulation models that do not resolve the wave motion. By

definition, the Stokes drift u_S is the difference between the Eulerian current u_E and the Lagrangian current u_L:

$$u_L = u_E + u_S \qquad (4)$$

The Stokes drift of surface gravity waves can be calculated from a numerical wave model (Breivik et al. 2016), by integrating over the entire directional wave spectrum. The magnitude of the Stokes drift is proportional to the third power of the frequency, which results in the wind-generated waves having a large contribution to the surface value. However, since Stokes drift decays exponentially with depth in proportion to wavelength, the Stokes drift due to swell decays more slowly with depth than the Stokes drift due to wind-generated seas.

An approximate Stokes drift profile can be calculated from the significant wave height, mean period and surface Stokes drift (Breivik et al. 2016). A further approximation is obtained from wind speed only, ignoring fetch limitations and contributions from swell and rapidly changing winds.

All objects and particles in the layer affected by wave motion – the Stokes layer – are subject to Stokes drift. Since particle transport in the open ocean is generally difficult to observe, the Stokes drift was a theoretical postulate at first. Monismith and Fong (2004) released dye in the open ocean and noted that the Stokes drift was the most likely mechanism to account for its observed trajectory. Röhrs et al. (2012) directly compared the movement of surface drifters with *in situ* measurements of the Eulerian current and the wave spectrum, and concluded that the Stokes drift was an essential part of the drifter trajectories. In this study, the Stokes drift of undrogued surface drifters was twice as large as their direct wind drag. Curcic et al. (2016) present drifter observations during the passage of a hurricane with substantial wave forcing and attribute major parts of the trajectories to Stokes drift. Tang et al. (2007) implemented both Stokes drift and associated wave-current interactions into an ocean model and a particle tracking model for surface drifters, which showed that the Stokes drift increased the drifter speeds by about 30% compared to neglecting its effect. This helped to decrease model errors for drifter trajectories significantly. Ardhuin et al. (2009) find that the Stokes drift contributes to the total surface current in the upper metre with 0.6–1.3% of the wind speed.

Momentum transfer between waves and currents

In addition to particle transport by Stokes drift, wave momentum and energy also affect the Eulerian ocean currents. Through wave growth, propagation and decay, the wave fields redistribute momentum and energy fluxes from the atmosphere (Longuet-Higgins 1953; Phillips 1977). In return, surface currents modify the wave field through wave refraction (Komen et al. 1994; Gemmrich and Garrett 2012).

During wave growth, the momentum flux from the atmosphere that goes into the wave field is not available to accelerate the surface current. During the onset of a storm, when waves are still growing, the momentum flux from winds into currents is thereby reduced by up to 10–30% (Perrie et al. 2003; Tang et al. 2007; Röhrs et al. 2012). Waves may then propagate over large distances and time before they release this momentum to the surface current through wave breaking (e.g. Perrie et al. 2003; Weber et al. 2006; Saetra et al. 2007).

A number of wave–current interactions occur on small scales, creating surface current patterns on scales at $\mathcal{O}(1\text{–}100\text{ m})$. Vertical shear of wind-induced currents and Stokes drift generate Langmuir circulation cells through tilting of vertical vorticity (Langmuir 1938). This results in convergence zones with strong downwind particle transport at the surface, which is important for e.g. oil spill transport (Simecek-Beatty and Lehr 2017). In shallow waters nearshore, waves can induce rip currents, which are return flows due to convergence of the wave induced mass transport induced by interactions with the bottom (Bowen 1969; Uchiyama et al. 2010).

The Coriolis-Stokes force

An analytical solution for the time-dependent response of the OSBL to forcing by both wind and waves is provided by Lewis and Belcher (2004), where Stokes drift becomes part in the momentum balance. Surface currents are oriented further to the right of the wind (northern hemisphere) than in the classic Ekman solution because the additional wave momentum effectively changes the surface boundary condition. An explanation is that the Coriolis force must be taken into account as a body force for the Lagrangian current; hence the Stokes drift itself is subject to the Coriolis force which accelerates an Eulerian current. This is commonly referred to as the Coriolis-Stokes force.

An effect of the Coriolis-Stokes force is to accelerate a current perpendicular to the Stokes drift. In a steady state, an Eulerian return flow that exactly opposes the Stokes drift is developed (Xu and Bowen 1994). This type of wave–current interaction can alter the direction of surface currents on time scales of several hours to a few days, dependent on the inertial period (e.g. Lewis and Belcher 2004). Observational evidence for the Coriolis-Stokes force is given by Christensen et al. (2018), who show that Stokes drift induces a surface current response
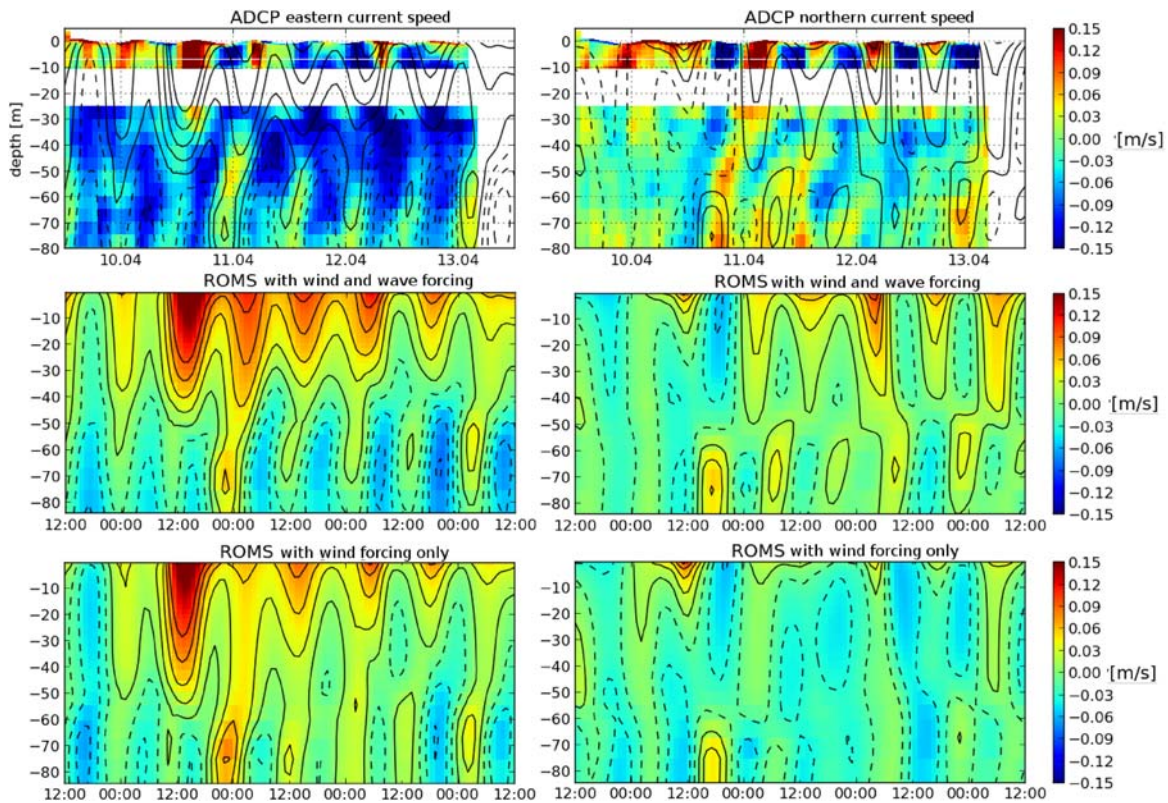
Figure 4. Hovmöller diagram of current data from ADCP measurements and from the ocean circulation model ROMS. The upper panels show data from a 1 MHz upward looking ADCP at 10 m depth (Röhrs et al. 2012) and a 500 kHz upward looking ADCP at 80 m depth (Fer and Paskyabi 2013) located in the semi-enclosed bay of Vestfjorden, Northern Norway. The lower panels show data from an ocean model that receives surface forcing from an atmospheric model only. The middle panel shows data from an ocean model that receives surface forcing from both an atmospheric model and a wave model, as outlined in Section 3.2. Both wave-induced surface stresses and the Coriolis-Stokes force are accounted for in this model. The contours of the middle panels are overlaid onto the ADCP data in the upper panels for comparison. The simulations show that the near-inertial wave that starts on 2011-04-10 12:00 is enhanced by the wave forcing. While the wave-induced stresses decrease the intensity of this wave (data not shown), the Coriolis-Stokes force greatly increases its intensity, providing a better fit to the ADCP observations at the surface and in deeper parts. The ocean model setup is described in (Röhrs et al. 2014).

similar to wind forcing, i.e. with deflection angle 90° to the right when forcing is exerted at the inertial frequency. An example of the effect of the Coriolis-Stokes force on surface currents is shown in Figure 4, depicting a situation where wave-current coupling in an ocean model enhances near inertial oscillations at the surface in accordance with observations from current meter.

3.3. Low-frequency currents

The large-scale ocean circulation, with spatial scales of $\mathcal{O}(10\text{–}1000\text{km})$, is approximately in geostrophic balance (Pedlosky 1987). The time-mean circulation is driven both by winds and by thermohaline forcing, the latter due to surface heating/cooling, evaporation, precipitation and freshwater fluxes. The circulation has complex spatial structure, being strongly influenced by the continental barriers and bathymetry. These engender intense currents near the western boundaries (e.g. the

Gulf Stream, Kuroshio and Agulhas currents) and also along eastern boundaries (e.g. the Norwegian, California and Leeuwin Currents) (e.g. Talley et al. 2011).

The boundary currents are without exception unstable, generating energetic mesoscale eddies with spatial scales comparable to the 'deformation radius' (typically 10–100 km) and temporal scales of days and longer. Variations in forcing (primarily the winds) also excite large-scale *planetary waves*, with spatial scales of 100–1000s of km and time scales of weeks to years. The waves propagate westward across ocean basins at speeds which vary with the square of the deformation radius, and can be seen in satellite observations of sea surface height (Chelton and Schlax 1996) and colour (Cipollini et al. 2001). Mesoscale eddies and planetary waves are usually surface-intensified and thus impact surface motion on sub-inertial time scales. The surface-intensification is a result of bathymetry limiting near-bottom flows (de La Lama et al. 2016; LaCasce 2017).

The mesoscale flows and the general circulation dominate transport at the surface on time scales longer than a day. Mesoscale particle dispersion is often interpreted in terms of turbulence theory (LaCasce 2008). The study of *relative dispersion*, involving the separation of pairs of particles, is particularly illuminating, as pair dispersion reflects the energetics on scales comparable to the pair separation. Richardson (1926) famously showed that the pair diffusivity (the time rate of change of the mean square pair separation) in the atmospheric boundary layer varies with separation to the 4/3 power. 'Richardson's Law' was subsequently found for particles and dye on the surface of lakes (Richardson and Stommel 1948) and the ocean (Okubo 1971). However, mesoscale eddy stirring can also produce very different dispersion, when the energy spectrum is dominated by the largest eddies. Under such *non-local* dispersion, pair separations increase exponentially in time. Such growth has been observed with separations below the deformation radius among surface drifters in the Gulf of Mexico, the Nordic Seas and in many other regions globally LaCasce and Ohlmann (2003); Koszalka et al. (2009); Corrado et al. (2017). Exponential dispersion is a characteristic of chaotic flows (Aref et al. 1990), implying a sensitive dependence on initial conditions. This directly impacts activities like search and rescue operations, because any error in the initial position will also grow exponentially in time.

Despite mesoscale eddies and planetary waves having weak bottom flows, they are nevertheless steered by bathymetry. This is evident from particle trajectories throughout the water column (Lacasce 2000). A striking example was seen in an experiment with acoustically-tracked floats in the western North Atlantic (Zhang et al. 2001); despite being within roughly 100 m of the surface, the floats did not spread east of the mid-Atlantic ridge, which lies over 1000 m below them.

Smaller scale eddies are also observed, with time scales nearer the inertial period and spatial scales of 100 m to 1 km. Such *submesoscale* eddies occur from instabilities in the mixed layer and near fronts (Thomas et al. 2008; McWilliams 2016). Due to their size and energetic nature, the eddies are significantly ageostrophic, with Rossby numbers exceeding one. The structures can affect surface dispersion, yielding local dispersion in addition to the non-local dispersion associated with mesoscale eddies (Corrado et al. 2017). Lateral convergences can also be large at such scales, as evidenced by drifters clustering near fronts (D'Asaro et al. 2018). Wind-forcing can also excite energetic inertial oscillations, causing drifters to cycle anticyclonically. However, despite enhancing particle energies, such isotropic motions have relatively little impact on dispersion (Beron-Vera and LaCasce 2016).

Such low frequency motions can significantly affect surface motion. Monitoring current variations on time scales of days to months is possible to some extent, if the observation systems are sufficient (Phillipson and Toumi 2017). But due to their chaotic nature, mesoscale and submesoscale eddies are generally difficult to predict (Nonaka et al. 2016).

4. Observations of surface currents

4.1. Eulerian current meter

Current meter are the primary tool for current observations for both industry site monitoring and long-term deployments for basic oceanographic research. Recording current anemometers were used in the 1900s to 1920s by Ekman and Helland-Hansen to provide point measurements of horizontal currents at depth, and later developments in the 1960s allowed for extended measurement periods using mechanical recording current meter (Ellingsen 2013). Today, Acoustic Doppler Current Profilers (ADCPs) allow currents to be profiled at high temporal resolution. ADCPs are typically mounted at fixed depths on a mooring or a structure, and measure currents over a range of 10–1000 m depending on their acoustic operating frequency (in the range of 40–1000 kHz). Higher frequencies allow better spatial resolution and accuracy, but shorter range.

Near-surface measurements using ADCPs remain a challenge. Errors are induced by wave orbital velocities, movement of the instrument, and back-scatter from the sea surface (e.g. Saunders 1976). Bruserud and Haver (2017) quantify uncertainties for current meter deployed on a surface following wave buoy, which increase with wave height. A range of physical explanations are suggested, including aliasing and bubbles.

Upward-looking ADCPs on a mooring line can be used to provide current measurements within centimetres of the surface under favourable conditions. An example of surface current data from two upward-looking ADCPs is shown in Figure 4, along with model data. In these experiments, a large floating buoy with an ADCP was mounted 10 m below the surface to keep the mooring line vertically taught in the presence of waves. Sentchev et al. (2017) obtain near-surface measurements from a floating platform, yielding currents up to 0.5 m below the surface. Laxague et al. (2018) also realised current measurements up to 0.2 m below the surface using an ADCP, and within 0.01 m using a polarimetric camera mounted below the surface.

Horizontal-looking ADCPs have been deployed from offshore platforms to provide near-surface currents, and downward-looking ADCPs are an established practice aboard surface vessels (Cooper et al. 2016). Vessel-based ADCP surveys cannot, however, resolve the upper few metres of the ocean and struggle to distinguish spatial structure from temporal evolution occurring during the survey. Such issues must be carefully evaluated in a given context, although they can be corrected to some extent in situations where evolution is a simple advection (e.g. when it is tidal, Dale et al. 2003).

4.2. Surface drifters

Surface drifters sample currents in a Lagrangian sense by largely following water parcels. Depending on their design, drifters are exposed to various degrees of wind- and wave forcing in addition to the Eulerian current for a specific depth range. Lumpkin et al. (2017) review the use and historical development of surface drifters to study dispersion and the upper ocean's wind response. Lagrangian measurements play a central role in the description of circulation statistics (e.g. Davis 1991; LaCasce 2008; Mariano et al. 2016).

Various instruments have been referred to as surface drifters in the recent literature, but they reflect the flow in different depth ranges. Drifters from the Surface Velocity Program (SVP), which employ a large holey-sock drogue at 15 m (Figure 1), are a standard for large-scale studies (Centurioni 2018). SVP drifters are not always useful for operational oceanography, however, because most floating objects are in the upper few metres. SVP data has nonetheless been useful for mapping currents, measuring dispersion and developing empirical models for the wind-driven Ekman layer (Rio et al. 2014; Elipot et al. 2016).

Shallower currents are commonly sampled using CODE-type drifters (Figure 1). The CODE drifter (Davis 1985) was designed to follow currents in the upper metre, with minimal contributions from wind and waves. It was recently re-designed to ensure minimal wind drag in controlled laboratory conditions and to meet requirements for large deployments, i.e. low-cost, environmentally sensitive and requiring minimum storage space on ships (Novelli et al. 2017).

Undrogued drifters, which are only partly submerged, have been used to investigate wind and wave effects on drifting objects. Poulain et al. (2009) have compared the drift of CODE drifters, drogued SVP drifters, and undrogued SVP drifters in the Mediterranean Sea to quantify wind-driven Ekman veering in the mixed layer. Spherical undrogued drifters (e.g. the

'iSphere' drifters) are specifically designed to mimic the drift of particular objects at the sea surface. Even more confined to the air–sea interface, thin bamboo plates can be used to measure currents in the upper few centimetres (Laxague et al. 2018) (Figure 1).

Since the advent of GPS positioning, drifter positions can be transmitted hourly or more frequently with a spatial accuracy of metres. This technological development provides a tool for real-time monitoring of surface currents and allows the study of high-frequency wind-driven surface currents and small scale eddies (e.g. Röhrs and Christensen 2015; Curcic et al. 2016; Mariano et al. 2016). If a drifter logs internally and is recovered, limitations on transmission bandwidth are avoided and temporal scales of seconds can be resolved. The key limitation is then the ability to appropriately seed a target region and the inherent bias towards undersampling of divergent/upwelling areas, accumulation of drifters in convergent/downwelling features such as fronts, or retention in eddies.

A major application of surface drifters has been to determine Lagrangian velocity and dispersion statistics, mostly using SVP drifters at 15 m depth (LaCasce and Bower 2000; Koszalka et al. 2009). With a sufficiently dense deployment, one is able to map Lagrangian characteristics over a given region. Some have questioned whether this is useful, since dispersion can vary so strongly in time (Mariano et al. 2016). Others suggest that persistent features can be found using climatological fields (Gough et al. 2019).

In operational oceanography, it is likely that using particle tracking models with real time velocities is preferred. Surface drifters provide the inherent advantage of directly measuring the surface velocities important for search and rescue (SAR) missions, the drift of large floating objects and oil-spill recovery. Surface drifters are therefore used during SAR missions to obtain now-casts of currents, provided a last-known position is available (Breivik et al. 2013). Attaching trackers to objects of particular interest has been used to estimate the leeway coefficient to improve trajectory prediction (Breivik et al. 2011).

4.3. Direct remote sensing

This section aims to provide a concise overview of direct remote sensing of surface currents, i.e. techniques that do not rely on models to translate from another observed quantity to surface currents. There are numerous, generally long established, indirect methods of inferring information about surface currents from satellite data, including geostrophic flow from surface height or feature tracking. As these rely to a large extent upon theoretical

oceanographic assumptions or models rather than direct measurement, they are described in Section 5.

HF radars

Surface current retrieval from land-based high frequency (HF) radars was developed in the 1970s and now plays a major role in operational oceanography (e.g. Rubio et al. 2017). Advantages are that (a) HF radars estimate spatial maps of time-variable currents in real-time, and (b) they provide estimates of the uppermost layer (Huang et al. 2017). HF radars emit radio waves at frequencies from 3 to 50 MHz, which are reflected through Bragg backscattering from surface gravity waves. The return signal experiences a Doppler shift by the apparent phase velocity of the scattering waves, which deviates from the phase velocity of the surface wave due to underlying surface current (Stewart and Joy 1974; Barrick and Weber 1977).

The choice of frequency for a HF radar systems requires to balance maximum range versus resolution. Frequencies of 30 MHz yield a range of 80 km at and a range resolution of about 1 km (Gurgel et al. 1999). HF radar applications are therefore restricted to coastal seas, and particular focus on near-shore and harbour currents require to chose VHF radars. Frequencies of 50 MHz achieve a range resolution up to 250 m but are restricted to 8km total range (e.g. Shay et al. 2002).

Because HF radar determines the current that a surface gravity wave experiences, the measurement represents an exponentially weighted average over the upper layer (Stewart and Joy 1974). The e-folding depth is related to the wavelength of the Bragg-scattering wave. For example, HF radars operating at 13.5 MHz use the Bragg scattering of 11.1 m long waves, giving an e-folding depth 0.88 m. This presents a method to estimate near-surface current shear when multiple frequencies are available, or by using secondary peaks in the backscatter signal (Shrira et al. 2001). Recent ADCP observations confirm the theoretical depth ranges of HF radar currents (Teague et al. 2001; Sentchev et al. 2017). Because of the measured depth range, suitable verification of HF radars is achieved using CODE-type drifters (Ohlmann et al. 2007; Rypina et al. 2014). However, HF radars provide Eulerian measurements and drifters measure the Lagrangian current. Therefore, differences due to Stokes drift must be considered during their comparison (Röhrs et al. 2015).

HF radars perform spatial and temporal averaging of surface currents. Depending on the operation frequency, typical grid cells are of the order of 1 km. Time averaging is usually over hourly intervals. This filtering in vertical, horizontal, and temporal domains presents a challenge when comparing HF radar currents with *in situ* data and explains most of the discrepancy between such data sets (Rypina et al. 2014).

A single HF radar antenna can only measure the component of the velocity in line with the antenna (Figure 5). Coastal observation systems therefore often consist of several HF radars, such that independent current components of neighbouring stations can be used to project both horizontal current components. Diagnostic models can be applied to fill regions of the radar domain that are covered by only one radar, assuming flow constraints such as convergence-free flow and tidal modes (Barrick et al. 2012). However, the quality of the estimated current components weakens as the intersecting beams of two radars become less perpendicular, a problem that is more pronounced along the coastline. Another approach to fill data gaps is to assimilate the radial currents into an ocean circulation model (e.g. Gopalakrishnan and Blumberg 2012), as performed by the model plotted in Figure 6.

Due to the complexity of the measurement principle, HF radar-based current data require careful interpretation. Nevertheless, HF radars have become one of the most important sources of surface current data in operational oceanography, because of their ability to cover extended areas. Below we give a few examples of the direct use of HF radar currents in operational oceanography. Warren et al. (2016) and Carvajal et al. (2016) describe the use of HF radar for validation of various satellite-derived surface current estimates. Heron et al. (2016) present the use of HF radars in coastal hazard management, including navigational safety, monitoring of suspended sediments during dredging and emergency response, as well as for Tsunami warning systems. Bellomo et al. (2015) discuss the use of HF radar networks for search and rescue and oil spill response.

Doppler centroid analysis from SAR

It has recently become possible to make direct measurements of ocean surface currents using Synthetic Aperture Radar (SAR). Techniques using conventional single antenna SAR data were pioneered by Chapron et al. (2005) and refined by Johannessen et al. (2008). An application to the Agulhas current was described by Rouault et al. (2010). The resulting Doppler Centroid Analysis (DCA) method was recently examined in detail for Envisat ASAR data by Hansen et al. (2011). The authors assess a number of limiting factors, anticipating improvements with the launch of new satellites.

The DCA exploits a Doppler shift due to the relative motion of the ocean surface along the line of sight of the side-looking SAR sensor. This includes the directional surface current component, but also a component
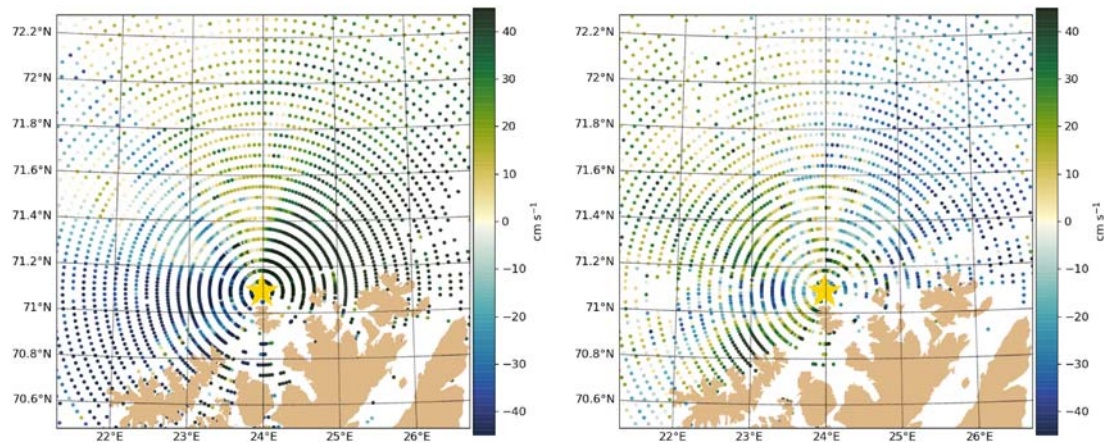
Figure 5. HF radar data from the Fruholmen station in Northern Norway. Colour-coded dots show surface current radials measured by a single antenna during 2019-03-24 03:00 (left) and 22:00 (right). The velocity component away from the radar is shown here. The site of the HF radar is indicated by a yellow star.

which is normally much larger due to the orbital motion of larger waves. This moves the shorter surface scattering facets and Bragg waves at orbital speed, with a net contribution along the wind/wave direction due to the effects of tilt and hydrodynamic modulations (Johannessen et al. 2008). It can be modelled, e.g. by an empirical correlation with wind (Mouche et al. 2012) and removed to extract the surface current from the total Doppler velocity. The uncertainty from a single SAR image is relatively large, due to a combination of the SAR sensor accuracy wave orbital velocity correction. The accuracy can be improved by averaging the Doppler Centroid over a larger area. A common compromise is to provide the Doppler current at a resolution of about 5–10 km, yielding an absolute uncertainty of

about 5–10 cm/s (Hansen et al. 2011). By averaging the directional current over several SAR images with similar orientations, temporal averages may be obtained with higher accuracy, and 2D current vector fields may also be reconstructed as in the example shown in Figure 7. As for HF radar, the effective measuring depth for the SAR Doppler is expected to be slightly below the ocean surface due to correlation between scattered velocity and wave phase. However, the exact depth is not known.

With typical satellite swath widths of 400 km, Doppler SAR images provide a larger overview than coastal HF-radars, and are also instantaneous snapshots of the ocean surface rather than temporal averages. The two main limitations are however the coarse and irregular
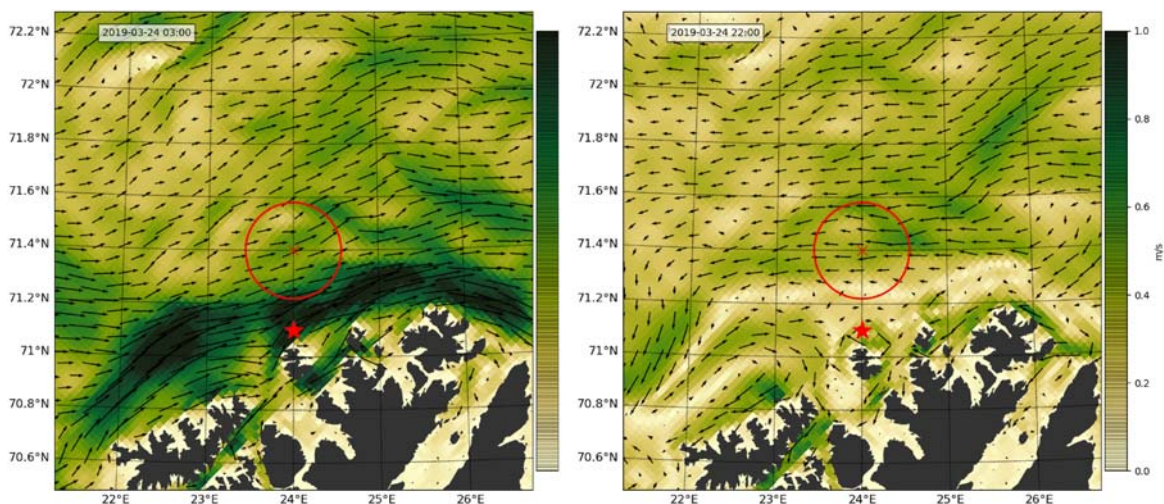
Figure 6. Surface current field at the coast off Northern Norway, as predicted from an operational ocean model (Röhrs et al. 2018b) for 2019-03-24 03:00 (left) and 22:00 (right). The ocean model with 2.4 km horizontal resolution assimilates HF radar current radials from the Fruholmen radar (center star). The same time steps as in Figure 5 are shown, indicating that major current features observed by the HF radar are represented in the model, and extended as full current vectors with coverage beyond the range of the radar station.
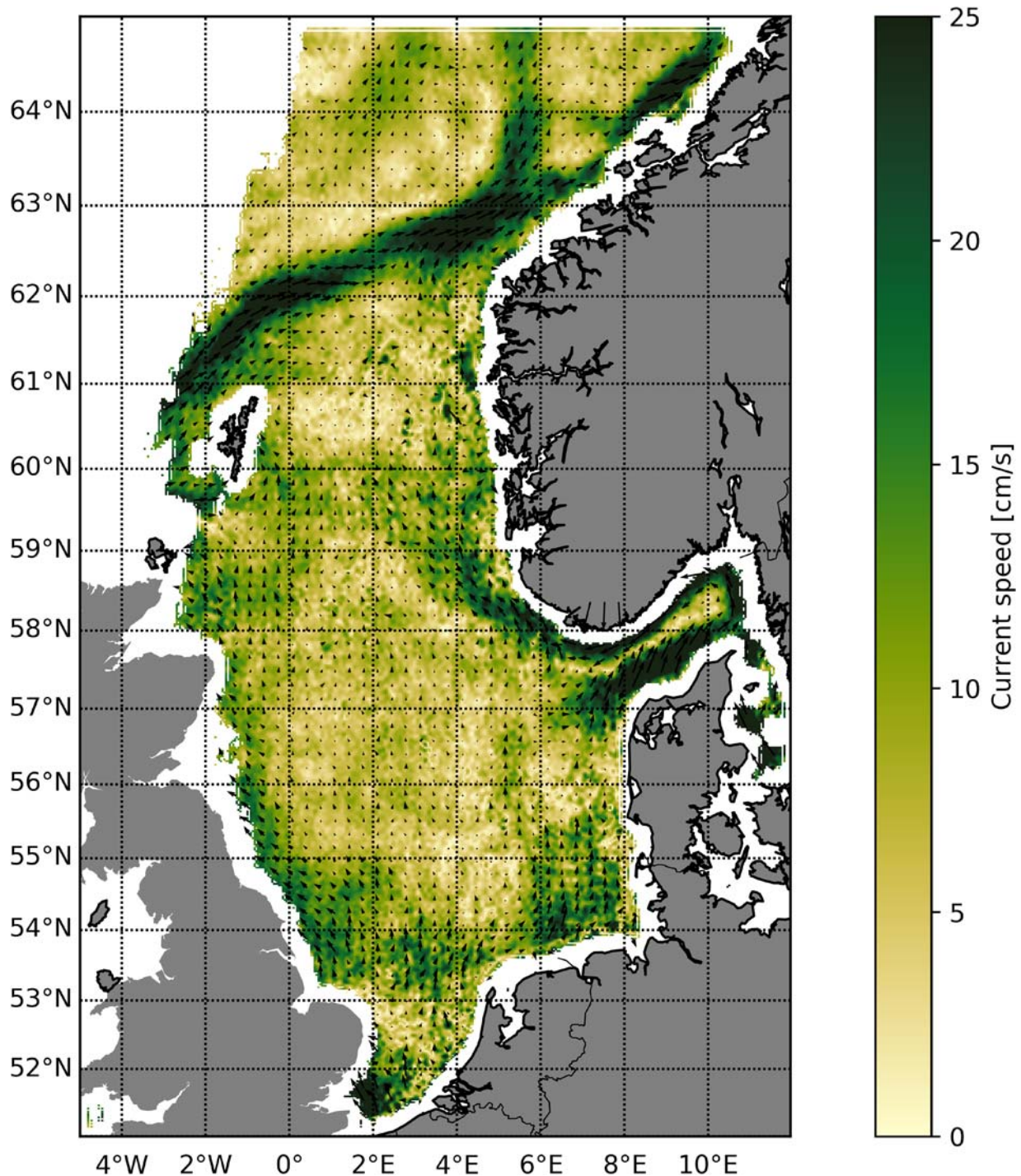
Figure 7. Total surface current retrieved by combining SAR Doppler velocity with geostrophic current from altimetry and gravimetry. Multiple SAR scenes within a time period of one month have been merged to create this current field. Reproduced from (Dagestad et al. 2013).

temporal resolution (satellite revisit time), and the fact that only the line-of-sight component of the current is detected. For this reason, the largest potential of the DCA method may lie in assimilation of this line-of-sight-component into operational models, or for scientific process studies. Whereas the spatial resolution of 5–10 km is finer than for satellite altimetry, it is still coarser than for HF-radar, and will be a limiting factor in detecting orographically steered current variations within fjords and bays and close to complex coastlines.

Along Track Interferometry
Along Track Interferometry (ATI) represents the main alternative to DCA for direct measurement of ocean

surface currents using SAR. A fundamental difference is the requirement of a second SAR antenna, allowing potentially superior accuracy and spatial resolution. Pioneering measurements were undertaken from aircraft by Goldstein and Zebker (1987), with the first application from orbit via the space shuttle described by Romeiser et al. (2005). The first satellite with ATI capability was TerraSAR-X launched in 2007, as described by Romeiser et al. (2010). Romeiser et al. (2014) compare DCA and ATI results, the latter originating from TerraSAR-X in isolation and in conjunction with its companion satellite TanDEM-X. The DCA and isolated TerraSAR-X ATI results were comparable, with the latter having some advantages. These achieved an accuracy of 0.1 m/s at about 1 km horizontal resolution. The best results were obtained from the combined TanDEM-X data, due to a short period of near optimal along track antenna separation (about 30 m for X band radar). An accuracy of 0.1 m/s was achieved with a resolution of about 33 m. ATI is also known as Along-Track Interferometric Synthetic Aperture Radar. A review of the technique was provided by Romeiser (2013). It must be noted that all of the SAR-based ocean surface current measurement techniques described above only provide the component of velocity along the line of sight. Two components of horizontal velocity can be derived from dual beam ATI systems, such as the aircraft mounted experimental system pioneered by Toporkov et al. (2005). Future mission concepts to provide this capability from satellites are being explored, e.g. the Wavemill concept described by Cotton et al. (2016).

Finally, regarding both DCA and ATI, it is also important to realise that the measured signal needs to be corrected for waves, which can be difficult to achieve reliably in some circumstances. Whereas ATI provides better spatial and numerical resolution than DCA, it is still limited by coarse and irregular revisit-time of the order of 1 day. Overall, the techniques represent an impressive development with great potential, but are not considered fully operational at this time. As for the DCA method, the largest potential may lie in assimilation of the line-of-sight current component into operational ocean models.

A notable recent innovation in airborne remote sensing of surface currents is the ROCIS system described by Cooper et al. (2016). This system, deployed from small aircraft, proved effective for monitoring the loop current and associated eddies in the Gulf of Mexico. ROCIS estimates surface currents from sequences of visual images of surface waves from a pair of rapidly sampling digital cameras. The system requires clear lines of sight to the ocean surface, i.e. cannot operate in cloudy conditions.

4.4. Satellite derivatives

Remote-sensing techniques that derive surface currents from observed fields by invoking a dynamical framework can be considered indirect, as opposed to the direct remote sensing techniques outlined in the previous section. This distinction follows the description of Isern-Fontanet et al. (2017). The dynamical frameworks rely upon analytical theory, sometimes supported by assumptions or measurements of other variables. They only provide estimates for specific components of the total current, while the direct methods reveal all components of the surface current. These methods are less applicable to coastal seas where satellite sensors suffer from interference with land, and higher resolution is often required.

Radar altimetry

The estimation of geostrophic currents via Sea Surface Height (SSH) from satellite altimeter has a long standing (e.g. Bernstein et al. 1982). To first degree, the SSH is equivalent to the earth's geoid and is highly correlated with seafloor variability. By combining all data collected over several years, models of the static geoid gradually improved (Marsh and Martin 1982). This allowed more accurate determination of the residual: the dynamic variation of the topography which is due to ocean circulation. Thus, under the assumption of geostrophically balanced large-scale currents, the current is inferred from the gradient of sea surface elevation. Le Traon et al. (2015) provides a summary of recent progress and future challenges. Jeans and Lefevre (2008) describe the successful industry application of altimeter-derived currents to quantify variability in Agulhas current impact at particular sites of interest. However they stressed how *in situ* measurement was critical for reliable quantification of current velocities, even in regions where geostrophic currents are very strong and dominant. In another industry application, Harrington-Missin et al. (2009) explained how altimeter-derived currents can provide valuable quantification of seasonal and interannual trends, complementing deficiencies in relatively short duration *in situ* measurements.

Inversion of the heat equation

Several methods have been devised that exploit dynamical frameworks to infer surface currents from satellite imagery (Isern-Fontanet et al. 2017). When image

sequences of sea surface temperature (SST) are available, conservation laws can be applied to obtain ocean currents. For instance, Chen et al. (2008) invert the heat conservation equation, which includes advection by currents, to quantify specific non-geostrophic components of the flow. This requires atmospheric heat fluxes from weather forecast models to account for local changes.

Surface quasi-geostrophic theory

Lapeyre and Klein (2006) and LaCasce and Mahadevan (2006) formulated a method to estimate sub-surface velocities of the mixed layer from single SST images based on surface quasi-geostrophic (SQG) theory. Herein, SST fields and assumptions about subsurface potential vorticity and stratification based on climatology are used to generate three dimensional flow fields. SQG extends classic quasi-geostrophic theory by prescribing the vertical structure, hence reducing degrees of freedoms. Compared with in situ measurements, the method provided plausible velocity estimate down to 50–100 m depth, that is primarily in the mixed layer (LaCasce and Mahadevan 2006). Lucas et al. (2012) found that the SQG method is well applicable for surface current nowcasting in operational oceanography. Wang et al. (2013) extended the method to include both SST and SSH data. This involved capturing two baroclinic modes and yielded realistic velocity predictions to roughly 1000 m depth. The method was simplified by LaCasce and Wang (2015), by using single hybrid baroclinic mode, referred to as a 'surface mode' (de La Lama et al. 2016; LaCasce 2017). Tandeo et al. (2016) describe an alternate method of combining SSH and SST data to estimate surface currents, exploiting co-variances between SSH and SST fields instead of a dynamical framework.

Maximum cross-correlation

Surface current estimation from SST, surface roughness or ocean colour are also possible through feature tracking in image sequences. The Maximum Cross-Correlation (MCC) method follow signatures of any observed quantity at the surface to obtain currents or surface drift, foremost applied to sea ice drift (e.g. Lavergne 2009). Warren et al. (2016) provide a recent example of surface currents estimated using MCC from ocean colour, evaluated using HF radar. Carvajal et al. (2016) describe a similar comparison of MCC-derived estimates with HF radar, two assimilated satellite products and four weather prediction models, noting some large differences.

Systematic sensor synergy

Retrieval methods for multiple sensors are combined to achieve better representations of various scales and processes. For example, Pascual et al. (2006) combine multiple altimeter missions to provide a gridded current product. The recent ESA GlobCurrent project (http://globcurrent.ifremer.fr/) aims to quantify distinct components of surface current using state-of-the-art satellite derivatives. These include the geostrophic currents, wind-driven Ekman, wave-driven stokes drift, tidal currents and internal wave-related surface currents (Johannessen et al. 2016). Rio et al. (2014) describe related work combining geostrophic and Ekman currents. GlobCurrent has some features in common with the NASA Ocean Surface Current Analyses-Real time (OSCAR) database (http://www.esr.org/oscar_index.html).

5. Ocean circulation and drift modelling

Numerical modelling techniques ultimately allow translation of physical understanding of ocean currents into data sets of ocean circulation. We will here describe the three main pillars that constitute numerical modelling in operational oceanography: general circulation models, data assimilation techniques and trajectory models.

5.1. Ocean general circulation models

Ocean general circulation models (OGCMs) provide continuous fields of ocean currents, temperature and salinity through discretisation of physical laws. These are conservation of momentum, conservation of mass, and the laws of thermodynamics (Griffies 2004; Roed 2018). Discretisation occurs horizontally on a scale of metres to kilometres, and vertically on a scale of centimetres to metres. Figure 6 shows an example of surface currents from an OGCM with 2.4 km horizontal resolution. This resolution permits the existence of baroclinc eddies, though their generation processes are not fully resolved.

Surface currents are simulated in OGCMs, but their level of detail is hampered by a few issues. The vertical resolution near the surface is often insufficient to capture all details of surface currents, particularly for the interfacial surface current of the upper centimetres. Even the direct wind-driven surface currents are not entirely resolved if atmosphere-ocean coupling occurs on too long time steps; generally hourly time coupling is required to resolve wind-driven currents in the upper metres (Elipot and Gille 2009b).

Horizontal resolution in models limits the degree to which baroclinic eddies are represented. Eddy-

permitting resolution (1–10 km) allows the existence of eddies but lacks detail of the physical mechanism that creates such instabilities. Eddy-resolving models should realistically capture baroclinic instabilities (Chassignet and Xu 2017; Sandery and Sakov 2017). A fair description of vertical stratification is important for how the upper ocean responds to wind forcing as well as for baroclinic instabilities and eddy generation (Pedlosky 1987).

Recent advancements in model coupling have improved the degree to which atmosphere-wave and wave-ocean interactions are represented in forecast models to describe momentum and energy balances at the surface (Section 3.2). Use of wave prediction models allow to calculate the parameters (eg. wave height, Stokes drift, wave energy dissipation) needed for model coupling (Komen et al. 1994). Jenkins (1989) were among the first documenting wave-ocean model coupling to account for wave-induced energy and momentum fluxes. Later frameworks also included Coriolis-Stokes forcing and Langmuir turbulence (Mellor 2005; Polton et al. 2005; Saetra et al. 2007; Ardhuin et al. 2008), however all of these methods use different formalism to derive wave-current interaction and may also produce differing results (Bennis et al. 2011). Wave and ocean models can be coupled online (e.g. Warner et al. 2008), or in an iterative fashion (e.g. Janssen 2012; Breivik et al. 2015). Both coupling strategies have been applied in operational services (e.g. Staneva et al. 2017; Lewis et al. 2019).

Improvements in atmosphere-wave-ocean coupling directly improves modelling of surface currents, particularly on short time scales as needed for drift modelling (e.g. Carniel et al. 2009; Curcic et al. 2016). Wave effects become particularly pronounced in the near-shore as gradients in radiation stresses from waves become larger near the coast (e.g. Uchiyama et al. 2010).

Using data from OGCMs, one also has to be aware that particular physical processes may be excluded in the model. In addition to insufficient coupling and outer model domain – wave models, hydrology for river run-off, and lateral model boundaries – bathymetry may be smoothed to ensure stability of the model system and some ocean models do not include tides because uncertainties in coastal bathymetry would lead to large errors in predicted tides (Egbert et al. 2004).

5.2. Data assimilation

Data assimilation (DA) is widely used in operational ocean modelling to adjust the initial model state to available observations (e.g. Sakov et al. 2012; Blockley

et al. 2014; Oke et al. 2015a; Tonani et al. 2015). Similarly, DA is used to reconstruct the ocean circulation of the past, i.e. reanalyses (e.g. Zuo et al. 2017; Carton et al. 2018). For a description of DA methods and applications in geosciences, we refer to Carrassi et al. (2018).

Assimilation of satellite altimetry is a long standing practise to constrain geostrophic large scale circulation patterns (Stammer and Griffies 2017). A newer approach is to directly assimilate observed currents, which has been shown to improve mesoscale circulation estimates (Oke et al. 2015b; Sperrevik et al. 2015). Improved vertical and horizontal water mass distribution through assimilation of SST and *in situ* observations of salinity and temperature also improve currents (e.g. Blockley et al. 2012; Oke et al. 2013; Sperrevik et al. 2017).

HF radars are the most common source for DA of remotely sensed surface currents (Isern-Fontanet et al. 2017). The ocean model depicted in Figure 6 assimilates the HF radar current radials shown in Figure 5, along with other observations. HF radar observations are limited to coastal areas, but their impact can be locally important even in global models and crucial in situations where forecasts are used for trajectory modelling for search-and-rescue (Breivik and Saetra 2001; Oke et al. 2015b). Sperrevik et al. (2015) provide an example of improved drift predictions from a regional model assimilating HF radar currents. Combined current vectors from multiple HF radars are commonly used for assimilation, but Barth et al. (2008) also provide an example of direct assimilation of radial velocities. This approach is appealing from a DA perspective, because observation errors for zonal and meridional current components in the derived total vectors are correlated and use of radial currents expands the range of HF radar observations.

In situ measurements of surface currents have been used for DA in a few studies. During the GLAD experiment in the Gulf of Mexico, ∼300 CODE-type surface drifters were deployed and Carrier et al. (2014) assimilated their velocities in the NCOM-4DVAR system and found substantial improvement in both analysis and forecast skill. Powell et al. (2008) assimilates ADCP observations from a moving vessel along with SST and SLA, and reports better fit to both the ADCP as well as to sea surface height, compared to an experiment in which the ADCP observations were not assimilated. Janeković et al. (2013) assimilates ADCP observations from four moorings deployed in shallow water on the coast of Oahu, and find significant error reduction in the along shore velocities. These examples illustrate the potential benefit from including current observations in DA systems.

Besides direct assimilation of drifter velocities, their information is also used to describe error co-variances as needed in data assimilation schemes (Jacobs et al. 2014a). This improves predictability for surface currents because variational data assimilation schemes require knowledge of model and observational uncertainties. Quantification of model errors presents a bottle neck in data assimilation routines (Moore et al. 2011) and forecasting (Vialard et al. 2005).

5.3. Trajectory models

The transport of objects in surface currents is relevant in many ecological and anthropogenic applications, and there is a growing number of models for different types of buoyant objects. van Sebille et al. (2018) reviews a range of aspects in Lagrangian particle modelling, and Zhang (2017) provides a review specific to marine plastic. A universal framework for trajectory modelling has been developed by Dagestad et al. (2018), which has been applied to oil spills, leeway modelling, plankton and marine plastic. Below, we discuss challenges associated with specific applications with operational significance. Common to all applications of near-surface trajectories is the difficulty of correctly describing the combination of current, wind and wave driven transport.

Floating objects, search-and-rescue
Predictions of the drift of buoyant objects is needed by a number of end users. On short but rapid timescales, the drift of boats, life rafts and persons in water is needed to guide search and rescue operations (Breivik et al. 2011). On longer timescales, location of debris from plane crashes (Carniel et al. 2002; Chen et al. 2012), stranded marine mammals (Haelters et al. 2006; Peltier et al. 2012), and the fate of macro plastics (Potemra 2012; Critchell et al. 2015) are reconstructed from trajectory models. A separate field of research focuses on ice-floes and icebergs (e.g. Smith 1993). The vertical extent of these objects determines from which depth ocean currents should be used in modelling.

Many larger objects are partly above water, hence they are also subject to direct wind drag. A difficulty in modelling is that the degree of submersion and hence the wind drag is often unknown. Separating the effects of wind, current and waves are crucial for drift modelling. Most commonly, the *leeway* is applied, defined as 'the velocity vector of the object relative to the downwind direction at the search object as it moves relative to the surface current as measured between 0.3 and 1.0 m depth caused by winds and waves' (Allen and Plourde 1999). Note that this definition targets a very specific depth, which is considered universal. The leeway is measured empirically in field trials using both current and wind measurements near the object. These measurements allow down- and cross-wind leeway coefficients to be determined by assuming a linear relationship (Breivik et al. 2011). This has been done for a wide range of different objects (e.g. Breivik et al. 2011; Brushett et al. 2014).

Wave-induced Stokes drift has been identified as a crucial component for transport near the ocean surface. For example, Stokes drift is primarily responsible for the beaching of objects (Carson et al. 2013; van den Bremer and Breivik 2018), as Eulerian ocean currents lack strong onshore currents near the coastline. The leeway method implicitly includes the Stokes drift under the assumption that surface gravity waves are in equilibrium with the wind forcing and that the mean depth of the object does not change with time as the Stokes drift decreases rapidly from the surface (Breivik and Allen 2008). Because wind and waves are not always aligned, as during the presence of swell, a more precise approach in trajectory modelling is to consider wind and Stokes drift separately. This has proven difficult because wind drag coefficients, as leeway coefficients, are obtained empirically. Users should always be aware of what mechanisms are included in empirical values to avoid double counting.

For very large objects (relative to wavelength of surface waves), there can be other wave forces acting in addition to Stokes drift. This is particularly relevant for ice floe modelling (Shen and Zhong 2001). Laboratory studies suggest that large flat objects which lie on the water surface might have higher than Stokes drift velocities (Huang et al. 2011; McGovern and Bai 2014) probably due to the effect of sliding (Grotmaack and Meylan 2006). Objects with a large vertical face can reflect or absorb wave energy directly (Smith 1993; Daniel et al. 2002).

Plankton transport
Plankton transport has a variety of applications such as prediction of harmful algal blooms (HABS) (Aleynik et al. 2016), ichthyoplankton pathways for fish stock recruitment (Feng et al. 2011; Gaspar et al. 2012) or spread of invasive species (Brickman 2014) and lice between fish farms (Gillibrand and Willis 2007; Adams et al. 2015). Predictions require accurate modelling of the entire surface layer, either because these particles are buoyant, or because biological behaviour such as diel vertical migration cause them to stay near the surface for prolonged periods (Gillibrand and Willis 2007). For

pelagic plankton, a description of turbulence is also needed to model their vertical distributions, so that currents at the correct depths are used for horizontal transport. For example, strong wind-induced turbulence enables a deeper penetration of particles in the water column, sheltering them from wind-induced currents and Stokes drift near the surface (Röhrs et al. 2014).

Plankton transport modelling for fish stock and aquaculture management can have an operational context if the results are used for time-critical decision-making. Vikebø et al. (2011) use a model for ichthyoplankton drift to assess fish stock recruitment of cod and herring, which is used to recommend quotas for maximum allowed catch for the ongoing season. Monitoring of lice spread between fish farms is used to determine impacts of expansion or reduction of salmon aquaculture on the Norwegian coast. Harmful algal blooms also require real-time modelling of plankton trajectories and growth.

Several model or experimental studies have highlighted that wave-induced transport is important for the transport of ichthyoplankton (Monismith and Fong 2004; Hrycik et al. 2013). Feng et al. (2011) found that inclusion of Stokes drift provided a mechanism for driving larvae onshore for recruitment within their model and produced a better match to observations.

Oil spill modelling

Oil spills can be modelled as Eulerian fields by solving the advection-diffusion equations (e.g. Sobey et al. 1997; Restrepo et al. 2015) or, more commonly, as Lagrangian particles (e.g. Daniel et al. 2003; De Dominicis et al. 2016; Röhrs et al. 2018a). Depending on the oil type, they are modelled as being on exactly the water surface or in the immediate subsurface (Giarrusso et al. 2001; Jones et al. 2016).

As well as the advective components of drift, oil spill models have components covering properties such as spreading, evaporation, dispersion and emulsification (Sebastião and Soares 2006) though Abascal et al. (2009) notes that the current field is the least developed part of operational systems. A percentage of wind speed is sometimes added to the advection of oil particles (Drivdal et al. 2014; Jones et al. 2016). This reflects the fact that the surface slick is much thinner than the uppermost layer of an OGCM and consequently experiences a higher degree of wind forcing.

Stokes drift is a pivotal mechanism for beaching of oil (Sobey et al. 1997; Röhrs et al. 2018a), and Stokes drift shear contributes to horizontal spreading on local scales (Elliott 1986). Many authors have pointed out that the contribution of waves to oil spill drift should be treated separately from wind drag (Lange and Hühnerfuss 1978; Sobey et al. 1997; Daniel et al. 2003). Explicitly including Stokes drift has improved some models (Castanedo et al. 2006; Jones et al. 2016) but not others (Abascal et al. 2009; Daniel et al. 2003). While the importance of Stokes drift for surface transport is undisputed, its implementation in transport models requires careful consideration as parts of the model system may already account for the Stokes drift through empirical relationships, such as universal wind drift factors or relationships between winds and currents. If Stokes drift is taken into account explicitly, a wind drift factor and current fields that do not include Stokes drift must be used.

6. Discussion

A survey of the literature from remote sensing, *in situ* experiments, and modelling studies shows that there are various views of surface currents which are partially incompatible. There are three aspects in which surface current descriptions differ: (i) depth range, (ii) time scale, and (iii) physical mechanisms that are accounted for. The depth ranges often differ because observation techniques sample at different depths. Time scales differ because observed and model data are always provided as average over a time period (Figure 2). Consideration of physical mechanisms differ between current products because indirect observation techniques and models are based on assumptions that necessarily leave out parts of the surface currents.

6.1. Spatio-temporal variability of surface currents

Surface currents can vary rapidly in space and time, therefore various definitions of surface currents give different results. As described in Section 3, there is a wide range of processes that generate and control the structure of surface currents, such as wind, waves, turbulence, tides, baroclinic instabilities, internal density gradients and barotropic pressure gradients. The total current is a result of all processes and nonlinear interaction between the various parts.

It is generally not possible to disentangle the currents created by various forcing mechanisms, but a few methods have been successfully used to isolate particular processes. For example, spectral decomposition allows identification of tidal currents and inertial oscillations (Pawlowicz et al. 2002). Temporal averaging allows isolation of steady-state Ekman currents on time scales longer than a few days (Gonella 1972), and spatial filtering allows identification of geostrophic

currents. Baroclinic eddies can be isolated using wavelet analysis of drifter trajectories (Lilly and Gascard 2006) or by studying Lagrangian coherent structures (Beron-Vera et al. 2008). Such techniques provide understanding of current mechanisms, and allow comparison of currents from various observation or modelling sources.

Applications in operational oceanography most commonly require coverage of short time scales, i.e. hours to days. In this context, directly wind-driven currents often dominate near the surface (compare Figure 4). Wind-driven inertial oscillations account for a major part of variability in surface currents on short time scales, judging from the peak in velocity spectra from GPS-tracked drifters (e.g. Poulain et al. 1992; Elipot and Gille 2009b; Röhrs and Christensen 2015) and HF radar-derived currents (e.g. Shrira et al. 2001; Ardhuin et al. 2009). Model or observational data sets that do not adequately resolve the local inertial frequency should be treated with caution if inertial timescales are important, as inertial oscillations may be aliased to considerably longer periods. For instance, when working with daily instantaneous model states, this problem is particularly severe when the inertial period is close to 24 h (30 deg of latitude) or 12 h (polar regions).

Applications in operational oceanography also need to consider the depth structure of currents in the upper few metres. Recent studies that focus on the upper metre show that there is considerable vertical shear in wind-driven situations (e.g. Sentchev et al. 2017) and particularly in the upper centimetre (Laxague et al. 2017). Ocean circulation models often do not resolve the shear in the upper centimetre (e.g. Warner et al. 2005) and remote-sensing techniques retrieve the current signature from a particular depth range or depth interval (Figures 2 and 3).

It is clear that any available information on surface currents, either stemming from models or measurements, contain inherent weaknesses. Models are limited by predictability and representation of physical regimes, and observations provide limited coverage in time and space. Synthesis of data sets can provide a more complete view than what is offered by a single data source. Synthesis between various surface current data is also necessary for calibration of algorithms, model validation and to assess measurement errors. Synthesis of data means that equivalent information is retrieved from data sets with different representations of surface currents.

6.2. Classification of depth ranges

We identify four depth ranges of surface currents that apply in operational oceanography (Table 2). They are covered by different observation techniques (Figure 2) and relate to different applications (Figure 3). Their definitions also directly relate to layers in boundary layer theory (Section 3.1).

The *interfacial surface current* refers to a region within millimetres of the sea surface. Several studies of drift at the ocean surface have pointed out that there is a downwind drift in the upper few centimetres that most circulation models do not account for, e.g. for oil slicks (Jones et al. 2016) and smaller marine debris. Laxague et al. (2018) confirmed such a layer with strong downwind drift from observations of flat Lagrangian drifters at the air–sea interface and refer to this part as the interface forcing layer. Reflecting their phrase, we suggest the term *interfacial surface current* for the current in the friction layer.

The *direct wind-driven current* refers to a depth of a few decimetres up to a few metres. In this regime, currents experience a direct acceleration by wind stress on a time scale of a few hours. This layer directly corresponds to the constant flux layer, distinguished by intermediate adjustment to forcing conditions and a logarithmic velocity profile under neutral stratification (O'Brien 1970). Observations indicating a distinction of this layer were provided by Sentchev et al. (2017), who show from ADCP measurements that only the upper 4 m were directly affected during sea breeze conditions, even under non-stratified conditions. Stokes drift affects particle transport in this depth range (van den Bremer and Breivik 2018) but should be considered separately from the direct wind-driven current.

The *surface boundary layer current* refers to the motion of the entire boundary layer, best represented by the Ekman layer. Changes occur on time scales longer than the inertial period (i.e. $\approx$12 h at a latitude of 50 deg). A local force balance is dominated by the Coriolis force, turbulent shear stress (vertical flux of horizontal momentum) and inertia. The depth-averaged current for the interior of the surface boundary layer has been extensively studied, e.g. using SVP drifters and depth-averaged theoretical models. A further distinction is possible between the steady-state and time-evolving surface boundary layer currents, i.e. steady-state Ekman current vs. inertial oscillations (Lewis and Belcher 2004). However, these are only distinguished by their time scale but occupy the same depth range.

An *effective drift current* is defined as the integrated current over a fixed depth range that is relevant for a specific application. This definition differs from the definitions above because it is not related to underlying geophysical mechanisms. However, an effective drift current is often needed for applications to floating

objects or the exposure of offshore structures (Table 1). Surface currents with such a specification are often referred to in the literature, and is requested from users for engineering purposes. To avoid confusion with terms for surface currents that are defined for typical layers or mechanisms, we suggest the term effective drift current. This definition does not depend on environmental conditions.

6.3. Predictability of surface currents

An upper limit of predictability in weather forecasts – that is how long ahead weather could theoretically be predicted using perfect models – originates from the chaotic nature of geophysical flow and uncertainties in the initial conditions (Lorenz 1982; Froude et al. 2013). The lower limit of predictability is the forecast skill of today's models. For ocean current forecast, this lower limit is far below the theoretical possible because the spatial scales associated with short time scales are not covered by observation systems, resulting in very poor initial conditions. In addition, data assimilation schemes also require a good description of the model's background error to adjust the model states according to the retrieved observations, which is usually not available on the scale of mesoscale ocean circulation (Jacobs et al. 2014a).

For mesoscale ocean circulation, it has not been established what the upper limit of predictability is, as opposed to the well known limit of 10 days in weather forecasting (Lorenz 1982). For oceanic predictability, most work on predictability has focused on climate and seasonal scales (e.g. Årthun and Eldevik 2016; Nonaka et al. 2016). Nevertheless, observation system experiments have shown that prediction of oceanic frontogenesis is possible when sufficient number of altimeter observations that determine the eddy field are available (Jacobs et al. 2014b).

It must also be expected that the various components of surface circulation should differ in their degree of predictability, as stated by E. Lorenz in his early studies on atmospheric predictability (Lorenz 1969). Sub-mesoscale eddies and baroclinic fronts must be considered to be the least predictable, because they are highly nonlinear and hence depend to a larger degree on initial values (Penduff et al. 2011). In contrast, tides and topographically steered currents are already predicted well by today's models.

Near inertial oscillations (NIOs), which occupy a large part of the surface variance spectrum of surface currents, have an ambiguous degree of predictability. modelling their exact onset, amplitude and phase has proven difficult because they critically depend on the details of air–sea coupling and ocean stratification. A small error in phase can lead to current vectors in opposite directions, and even numerical artefacts from the air–sea coupling scheme may trigger artificial NIOs. However, inertial oscillations are not subject to the initial value problem associated with intrinsic non-linearity, because they foremost depend on ocean stratification and wind history, which are more predictable. A criterion for the onset of NIOs, using a wavelet transform of wind history, has been put forward by Christensen et al. (2018).

Wind-driven ocean circulation on time scales larger than the inertial period are considered to be well predictable by current models, given a fair predictability of wind and pressure fields from numerical weather models (Nonaka et al. 2016). The lower frequency components of surface flow also have smaller differences in the vertical and are hence easier to apply. Owing to their dependence on wind forcing, global ocean models are generally considered more reliable for ocean currents at the surface than at depth (e.g. Jeans et al. 2014).

An important tool to deal with the chaotic nature of geophysical flow and model uncertainty are ensemble prediction systems. Ensemble prediction has revolutionised numerical weather prediction in the 1990s (Gneiting and Raftery 2005) and may assume a similar role in oceanography. Ensemble predictions have been adopted in seasonal ocean forecasting (Williamson et al. 2013), e.g. to predict the probability of El-Nino onset (Xue et al. 2017) and have also been used in prediction of mesoscale eddy fields (Rixen et al. 2009; Nonaka et al. 2016). Ensemble methods are, furthermore, used to guide data assimilation schemes (e.g. Xie et al. 2017; Pasmans and Kurapov 2019).

6.4. A format for surface current forecasts

The uncertainties described above have bearing on a new facet of operational oceanography, i.e. that current forecasts be usable by users that are not specialists in physical oceanography. Similarly in weather forecasts, a probability of rainfall is often given because this parameter is difficult to predict precisely at a fixed location, but users still benefit from an outlook for the range of possibilities. In surface current forecasting, site-specific predictions are seldom useful because the focus on a single point is too susceptible to the variability from sub-mesoscale activity, as for rainfall events. Communication of the uncertainty is a priority, but predictable aspects of surface currents – tides, wind-driven, and geostrophic current – should
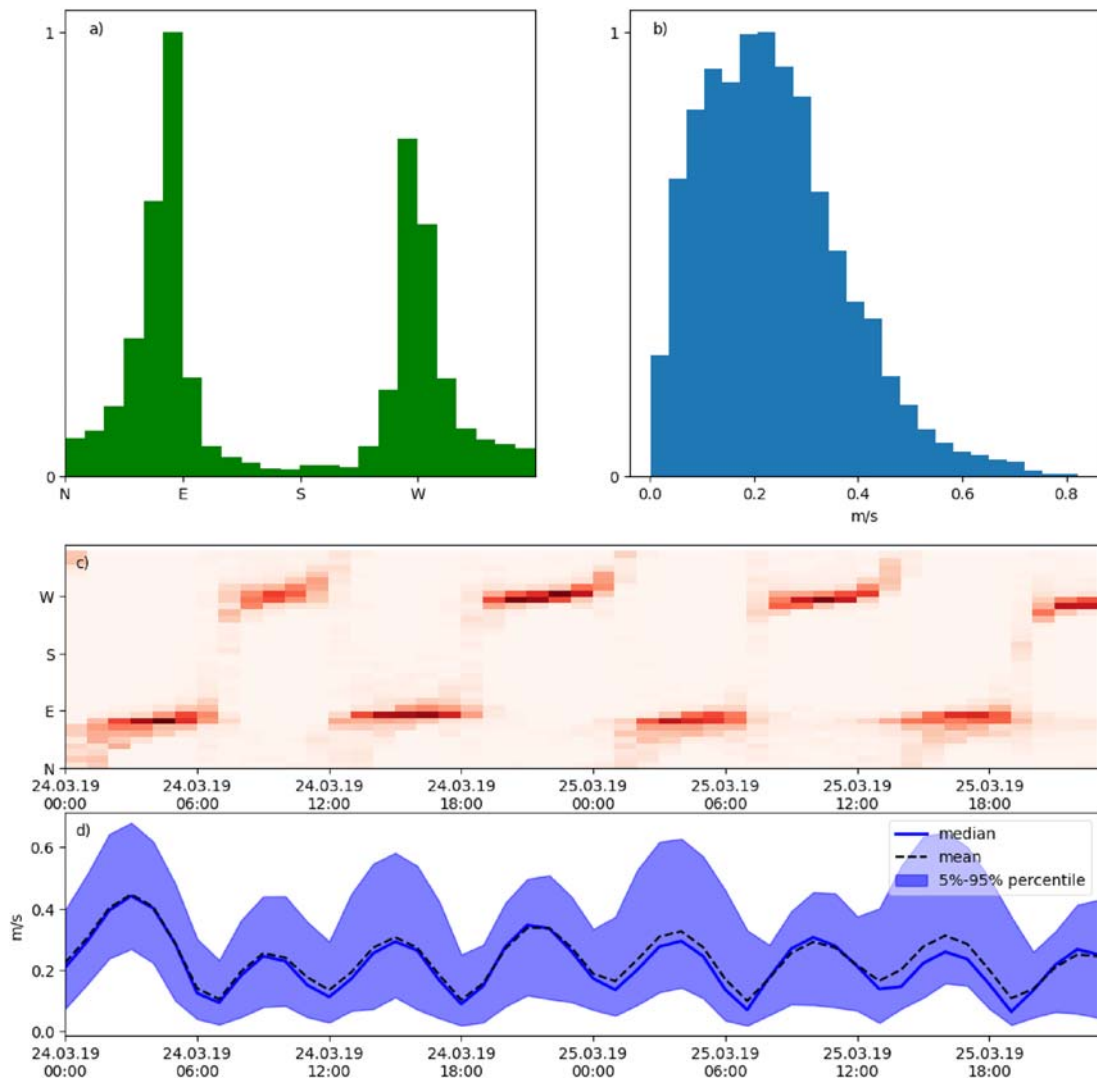
Figure 8. Example of how a surface current forecast for the situation in Figure 6 is presented to potential users. Panels (a) and (b) show 2D-histograms of surface current speed and direction for a 48 h time interval in the region encircled in Figure 6. Panel (c) shows directional occurrence frequency as a function of time within the forecast interval. Panel (e) shows statistics of total current speed as function of time within the forecast interval. This presentation highlights the most predictable parts of the surface current and omits detail of the parts that are not predictable, with focus on the possible variations in a representative region.

also be given attention in a useful format of surface current forecasts.

A statistical view on the spatial and temporal variability at present state can highlight the valuable information content of an ocean model forecast. Figure 8 is an example of a current forecast for the encircled region in Figure 6. The model data shown in Figure 6 is also animated in an electronic supplement for the duration of 48 h. The scene includes a strong coastal current, which is topographically steered and partly in geostrophic balance, and should hence have predictable components. There is also mesoscale activity with poor predictability.

The data presented in Figure 8 includes all model grid points within the circle in Figure 6 for a time period

of 48 h, which is the time scope of a hypothetical forecast in this case. The histograms in Figure 8(a,b) highlight the prevalence of strong northeastward and westward currents in the region, which are the result of the coastal jet current as well as tides. The time-dependent direction histogram in Figure 8(c) also shows when each tidal phase is to be expected. Together with the time series of total current speed in Figure 8(d), one can infer that the strongest currents are up to 0.6 m/s and in northeasterly direction in the selected region. Figure 6 indicated that the extreme current speeds should be expected in the southern part of the encircled region due to the coastal jet. This information can be extracted from the model data despite the existence of unpredictable mesoscale features.

Since operational applications require data on time scales of hours to days, wind-driven currents and tides exhibit a major relevance in operational oceanography. Since these are predictable, a useful forecast of surface currents can be issued by separating predictable components from other parts, i.e. mesoscale features. In addition, the low-frequency geostrophic flow is a matter of now-casting, already provided in operational context.

Acknowledgments

Disclosure statement

No potential conflict of interest was reported by the author(s).

Funding

Notes on contributors

Johannes Röhrs, meteorologist and physical oceanographer, works as scientist at the Norwegian Meteorological Institute. His work includes drift modelling and ocean modelling focusing on ensemble prediction and data assimilation methods. His recent research projects deal with upper ocean dynamics and consequences for tracer transport at the ocean surface.

Graig Sutherland is a senior scientist in Physical Oceanography who specializes in the drift and dispersion of material in the ocean. He also studies air-sea interaction and turbulent processes in the near-surface of the ocean.

Dr. Gus Jeans is an independent metocean consultant and professional oceanographer, with experience in academia and industry. Most of his work involves analysis and characterisation of ocean currents or offshore winds.

Michael Bedington is a numerical modeller whose work focuses on applied problems in coastal oceanography, using hydrodynamic, lagrangian, and biogeochemical models. He works on a variety of topics including HAB monitoring, water quality, coastal risk, and land-ocean carbon exchange.

Ann Kristin Sperrevik is a physical oceanographer, whose work is focused on operational oceanography and data assimilation.

Dr. Knut-Frode Dagestad is a researcher at the Norwegian Meteorological Institute, where he is responsible for research, development and implementation of ocean drift services. He is the main developer of the OpenDrift software.

Yvonne Gusdal is a physical oceanographer at the Norwegian Meteorological Institute who works with validation of operational ocean models to assess its general quality. She also has an interest in scientific visualization for presenting and understanding scientific data.

Cecilie Mauritzen, a senior scientist at the Norwegian Meteorological Institute, is an experimental physical oceanographer by training. Her recent projects range from the use of system dynamics to create learning environments for the climate system to the use of machine learning to model turbulence. She has been a Lead Author for IPCC's 4th and 5th Assessment Reports.

Andrew Dale is a lecturer in Physical Oceanography whose work spans observational dynamical oceanography and modelling. His recent work has included dispersive and transport studies in environments from coastal aquaculture to the deep sea.

Joe LaCasce is a professor in Physical Oceanography, whose research is focused on the dynamics of large scale motion. He also studies the theory of turbulent dispersion and has applied that to analyzing data from ocean drifters and floats.

ORCID

Johannes Röhrs ⓘ http://orcid.org/0000-0001-8402-2925
Graig Sutherland ⓘ http://orcid.org/0000-0001-6109-9022
Michael Bedington ⓘ http://orcid.org/0000-0002-4255-9406
Ann Kristin Sperrevik ⓘ http://orcid.org/0000-0003-3667-7913
Knut-Frode Dagestad ⓘ http://orcid.org/0000-0002-0412-7485
Cecilie Mauritzen ⓘ http://orcid.org/0000-0001-5956-8811
Joseph H. LaCasce ⓘ http://orcid.org/0000-0001-7655-5596

References

Abascal AJ, Castanedo S, Medina R, Losada IJ, Alvarez-Fanjul E. 2009. Application of HF radar currents to oil spill modelling. Mar Pollut Bull. 58(2):238–248.

Adams TP, Proud R, Black KD. 2015. Connected networks of sea lice populations: dynamics and implications for control. Aquac Environ Interact. 6(3):273–284.

Agrawal Y, Terray E, Donelan M, Hwang P, Williams AJ, Drennan W, Kahma K, Krtaigorodskii S. 1992. Enhanced dissipation of kinetic energy beneath surface waves. Nature. 359(6392):219–220.

Aleynik D, Dale AC, Porter M, Davidson K. 2016. A high resolution hydrodynamic model system suitable for novel harmful algal bloom modelling in areas of complex coastline and topography. Harmful Algae. 53:102–117.

Alford MH, Gregg MC. 2001. Near-inertial mixing: modulation of shear, strain and microstructure at low latitude. J Geophys Res. 106(C8):16947–16968.

Allen A, Plourde JV. 1999. Review of leeway: field experiments and implementation. Groton (CT): Coast Guard Research and Develepment Center. Technical Report CG-D-08-99.

Ardhuin F, Marie L, Rascle N, Forget P, Roland A. 2009. Observation and estimation of Lagrangian, Stokes, and Eulerian currents induced by wind and waves at the sea surface. J Phys Oceanogr. 39(11):2820–2838.

Ardhuin F, Rascle N, Belibassakis KA. 2008. Explicit wave-averaged primitive equations using a generalized Lagrangian mean. Ocean Model. 20(1):35–60.

Aref H, Stuart JT, Tabor M. 1990. Chaotic advection of fluid particles. Philos Trans R Soc London Ser A Phys Eng Sci. 333(1631):273–288.

Årthun M, Eldevik T. 2016. On anomalous ocean heat transport toward the arctic and associated climate predictability. J Clim. 29(2):689–704.

Barrick D, Fernandez V, Ferrer MI, Whelan C, Breivik O. 2012. A short-term predictive system for surface currents from a rapidly deployed coastal HF radar network. Ocean Dynam. 62:725–740.

Barrick DE, Weber BL. 1977. On the nonlinear theory for gravity waves on the ocean's surface. part II: interpretation and applications. J Phys Oceanogr. 7 (1):11–21.

Barth A, Alvera-Azcárate A, Weisberg RH. 2008. Assimilation of high-frequency radar currents in a nested model of the West Florida shelf. J Geophys Res Oceans. 113(C8).

Bellomo L, Griffa A, Cosoli S, Falco P, Gerin R, Iermano I, Kalampokis A, Kokkini Z, Lana A, Magaldi MG, et al. 2015. Toward an integrated HF radar network in the mediterranean sea to improve search and rescue and oil spill response: the TOSCA project experience. J Oper Oceanogr. 8(2):95–107.

Bennis A-C, Ardhuin F, Dumas F. 2011. On the coupling of wave and three-dimensional circulation models: choice of theoretical framework, practical implementation and adiabatic tests. Ocean Model. 40:260–272.

Bernstein RL, Born GH, Whritner RH. 1982. SEASAT altimeter determination of ocean current variability. J Geophys Res Oceans. 87:3261–3268.

Beron-Vera FJ, LaCasce JH. 2016. Statistics of simulated and observed pair separations in the gulf of Mexico. J Phys Oceanogr. 46(7):2183–2199.

Beron-Vera FJ, Olascoaga MJ, Goni GJ. 2008. Oceanic mesoscale eddies as revealed by Lagrangian coherent structures. Geophys Res Lett. 35(12).

Blockley EW, Martin MJ, Hyder P. 2012. Validation of foam near-surface ocean current forecasts using lagrangian drifting buoys. Ocean Sci. 8(4):551–565.

Blockley EW, Martin MJ, McLaren AJ, Ryan AG, Waters J, Lea DJ, Mirouze I, Peterson KA, Sellar A, Storkey D. 2014. Recent development of the met office operational ocean forecasting system: an overview and assessment of the new Global FOAM forecasts. Geosci Model Dev. 7 (6):2613–2638.

Bowen AJ. 1969. Rip currents 1: theoretical investigations. J Geophys Res. 74:5467–5478.

Breivik O, Allen AA. 2008. An operational search and rescue model for the Norwegian sea and the North sea. J Marine Syst. 69(1-2):99–113.

Breivik O, Allen A, Maisondieu C, Olagnon M. 2013. Advances in search and rescue at sea. Ocean Dynam. 63:83–88.

Breivik O, Allen AA, Maisondieu C, Roth JC. 2011. Wind-induced drift on objects at sea: the Leaway field method. Appl Ocean Res. 33:100–109.

Breivik O, Bidlot J-R, Janssen PA. 2016. A Stokes drift approximation based on the Phillips spectrum. Ocean Model. 100:49–56.

Breivik O, Mogensen K, Bidlot J-R, Balmaseda MA, M. Janssen PAE. 2015. Surface wave effects in the NEMO ocean model: forced and coupled experiments. J Geophys Res Oceans. 120(4):2973–2992.

Breivik O, Saetra O. 2001. Real time assimilation of HF radar currents into a coastal ocean model. J Mar Syst. 28 (3):161–182.

Brickman D. 2014. Could ocean currents be responsible for the west to east spread of aquatic invasive species in Maritime Canadian waters? Mar Pollut Bull. 85:235–243.

Bruserud K, Haver S. 2017. Uncertainties in current measurements in the Northern North sea. J Atmos Ocean Technol. 34(4):855–876.

Brushett BA, Allen AA, Futch VC, King BA, Lemckert CJ. 2014. Determining the leeway drift characteristics of tropical Pacific island craft. Appl Ocean Res. 44:92–101.

Carniel S, Umgiesser G, Sclavo M, Kantha LH, Monti S. 2002. Tracking the drift of a human body in the coastal ocean using numerical prediction models of the oceanic, atmospheric and wave conditions. Sci Justice. 42 (3):143–151.

Carniel S, Warner J, Chiggiato J, Sclavo M. 2009. Investigating the impact of surface wave breaking on modeling the trajectories of drifters in the northern Adriatic Sea during a wind-storm event. Ocean Model. 30(2-3):225–239.

Carrassi A, Bocquet M, Bertino L, Evensen G. 2018. Data assimilation in the geosciences: an overview of methods, issues, and perspectives. Wiley Interdiscip Rev Clim Change. 9(5):e535.

Carrier MJ, Ngodock H, Smith S, Jacobs G, Muscarella P, Ozgokmen T, Haus B, Lipphardt B. 2014. Impact of assimilating ocean velocity observations inferred from lagrangian drifter data using the ncom-4dvar. Mon Weather Rev. 142 (4):1509–1524.

Carson HS, Lamson MR, Nakashima D, Toloumu D, Hafner J, Maximenko N, McDermid KJ. 2013. Tracking the sources and sinks of local marine debris in Hawai'i. Mar Environ Res. 84:76–83.

Carton JA, Chepurin GA, Chen L. 2018. Soda3: a new ocean climate reanalysis. J Clim. 31(17):6967–6983.

Carvajal GK, Wozniak M, Heuzé C, Eriksson LEB, Johan K, Rydberg B. 2016. Assessment of satellite and ground-based estimates of surface currents. In: 2016 IEEE International Geoscience and Remote Sensing Symposium (IGARSS), Beijing. p. 4675–4678.

Castanedo S, Medina R, Losada IJ, Vidal C, Méndez FJ, Osorio A, Juanes JA, Puente A. 2006. The prestige oil spill in Cantabria (Bay of Biscay). Part I: operational forecasting system for quick response, risk assessment, and protection of natural resources. J Coast Res. 226:1474–1489.

Centurioni LR. 2018. Drifter technology and impacts for sea surface temperature, sea-level pressure, and ocean circulation studies. In: Venkatesan R, Tandon A, D'Asaro E, and Atmanand MA, editors. Observing the oceans in real time. Cham: Springer International Publishing. p. 37–57. (Springer oceanography).

Chapron B, Collard F, Ardhuin F. 2005. Direct measurements of ocean surface velocity from space: interpretation and validation. J Geophys Res Oceans. 110(C7):C07008.

Chassignet EP, Verron J, editors. 2006. Ocean weather fore-casting: an integrated view of oceanography. Springer Netherlands. https://www.springer.com/gp/book/9781402 039812

Chassignet EP, Xu X. 2017. Impact of horizontal resolution on gulf stream separation, penetration, and variability. J Phys Oceanogr. 47(8):1999–2021.

Chelton DB, Schlax MG. 1996. Global observations of oceanic Rossby waves. Science. 272(5259):234–238.

Chelton DB, Schlax MG, Samelson RM, Szoeke RAD. 2007. Global observations of large oceanic eddies. Geophys Res Lett. 34(15).

Chen C, Limeburner R, Gao G, Xu Q, Qi J, Xue P, Lai Z, Lin H, Beardsley R, Owens B, et al., members of the UMASS-D FVCOM Group and and members of the WHOI Field Measurement Group. 2012. FVCOM model estimate of the location of Air France 447. Ocean Dyn. 62(6):943–952.

Chen W, Mied RP, Shen CY. 2008. Near-surface ocean vel-ocity from infrared images: global optimal solution to an inverse model. J Geophys Res Oceans. 113(C10).

Christensen KH, Breivik O, Dagestad KF, Röhrs J, Ward B. 2018. Short-term prediction of oceanic drift. Oceanography. 31:59–67.

Cipollini P, Cromwell D, Challenor PG, Raffaglio S. 2001. Rossby waves detected in global ocean colour data. Geophys Res Lett. 28(2):323–326.

Cooper C, Danmeier D, Frolov S, Stuart G, Zuckerman S, Anderson S, Sharma N. 2016. Real time observing and fore-casting of loop currents in 2015. In: Offshore Technology Conference. Houston (TX): Offshore Technology Conference. p. 16.

Corrado R, Lacorata G, Palatella L, Santoleri R, Zambianchi E. 2017. General characteristics of relative dispersion in the ocean. Sci Rep. 7(1):46291.

Cotton PD, Gommenginger C, Martin A, Marquez J, Burbidge G, Quilfen Y, Chapron B, Reppucci A, Buck C. 2016. Wavemill product assessment- defining products and evaluating potential performance from a novel space-borne interferometric SAR. In: *Proceedings of the Conference*; Vol. 740; Prague, Czech Republic. p. 64.

Craig PD, Banner ML. 1994. Modeling wave-enhanced turbu-lence in the ocean surface layer. J Phys Oceanogr. 24 (12):2546–2559.

Crawford GB, Large WG. 1996. A numerical investigation of resonant inertial response of the ocean to wind forcing. J Phys Oceanogr. 26:873–891.

Critchell K, Grech A, Schlaefer J, Andutta FP, Lambrechts J, Wolanski E, Hamann M. 2015. Modelling the fate of mar-ine debris along a complex shoreline: lessons from the Great Barrier Reef. Estuar Coast Shelf Sci. 167:414–426.

Curcic M, Chen SS, Özgökmen TM. 2016. Hurricane-induced ocean waves and stokes drift and their impacts on surface transport and dispersion in the Gulf of Mexico. Geophys Res Lett. 43(6):2773–2781.

Dagestad K-F, Hansen MW, Johannessen JA, Chapron B. 2013. INCUSAR–a method to retrieve temporal averages of 2D ocean surface currents from synthetic aperture radar doppler shift. In: Fernández-Prieto D, Sabia R, edi-tors. Remote sensing advances for earth system science: The esa changing earth science network: projects 2009–2011. Berlin, Heidelberg: Springer. p. 59–67. (SpringerBriefs in earth system sciences).

Dagestad K-F, Röhrs J. 2019. Prediction of ocean surface tra-jectories using satellite derived vs. modeled ocean currents. Remote Sens Environ. 223:130–142.

Dagestad K-F, Röhrs J, Breivik O, Ådlandsvik B. 2018. OpenDrift v1.0: a generic framework for trajectory model-ling. Geosci Model Dev. 11(4):1405–1420.

Dale AC, Ullman DS, Barth JA, Hebert D. 2003. The front on the Northern Flank of Georges bank in spring: 1. Tidal and subtidal variability. J Geophys Res Oceans. 108(C11).

Daniel P, Jan G, Cabioc'h F, Landau Y, Loiseau E. 2002. Drift modeling of cargo containers. Spill Sci Technol B. 7(5-6):279–288.

Daniel P, Marty F, Josse P, Alain R, Bp C, Skandrani C, Benshila R, Alain R, Bp C. 2003. Improvement of drift cal-culation in MOTHY operational oil spill prediction system. In: Internation Oil Spill Conference, Vancouver, British Columbia, Canada. p. 1–6.

D'Asaro EA. 1985. The energy flux from the wind to near-inertial motions in the surface mixed layer. J Phys Oceanogr. 15(8):1043–1059.

D'Asaro EA, Eriksen C, Levine M, Niiler P, Paulson C, Vanmeurs P. 1995. Upper-ocean inertial currents forced by a strong storm.1. Data and comparisons with linear-the-ory. J Phys Oceanogr. 25(11):2909–2936.

D'Asaro EA, Shcherbina AY, Klymak JM, Molemaker J, Novelli G, Guigand CM, Haza AC, Haus BK, Ryan EH, Jacobs GA, et al. 2018. Ocean convergence and the dispersion of flotsam. Proc Natl Acad Sci. 115 (6):1162–1167.

Davis RE. 1985. Drifter observations of coastal surface cur-rents during code: the method and descriptive view. J Geophys Res. 90(C3):4741–4755.

Davis RE. 1991. Observing the general circulation with floats. Deep Sea Res A Oceanogr Res Papers. 38:S531–S571.

De Dominicis M, Bruciaferri D, Gerin R, Pinardi N, Poulain PM, Garreau P, Zodiatis G, Perivoliotis L, Fazioli L, Sorgente R, et al. 2016. A multi-model assessment of the impact of currents, waves and wind in modelling surface drifters and oil spill. Deep-Sea Res Pt II. 133(Supplement C):21–38.

de La Lama MS, LaCasce JH, Fuhr HK. 2016. The vertical structure of ocean eddies. Dyn Statist Clim Syst. 1(1).

Drivdal M, Broström G, Christensen KH. 2014. Wave-induced mixing and transport of buoyant particles: application to the Statfjord A oil spill. Ocean Sci. 10 (6):977–991.

Egbert GD, Ray RD, Bills BG. 2004. Numerical modeling of the global semidiurnal tide in the present day and in the last glacial maximum. J Geophys Res Oceans. 109(C3).

Ekman VW. 1905. On the influence of the earth's rotation on ocean-currents. Arkiv f Mat Astr o Fys. 2(11).

Elipot S, Gille ST. 2009a. Ekman layers in the southern ocean: spectral models and observations, vertical viscosity and boundary layer depth. Ocean Sci. 5:115–139.

Elipot S, Gille ST. 2009b. Estimates of wind energy input to the Ekman layer in the Southern ocean from surface drifter data. J Geophys Res Oceans. 114:C06003.

Elipot S, Lumpkin R, Perez RC, Lilly JM, Early JJ, Sykulski AM. 2016. A global surface drifter data set at hourly resol-ution. J Geophys Res Oceans. 121(5):2937–2966.

Ellingsen G. 2013. Varme havstrømmer og kald krig. "Bergensstrømmåleren" og vitenskapen om havstrømmer

fra 1870-årene til 1960-årene [PhD thesis]. Bergen: University of Bergen.

Elliott AJ. 1986. Shear diffusion and the spread of oil in the surface layers of the North Sea. D Hydrogr Z. 39 (3):113–137.

Feng M, Caputi N, Penn J, Slawinski D, de Lestang S, Weller E, Pearce A. 2011. Ocean circulation, Stokes drift, and connectivity of western rock lobster (Panulirus cygnus) population. Can J Fish Aquat Sci. 68(7):1182–1196.

Fer I, Paskyabi MB. 2013. Autonomous ocean turbulence measurements using shear probes on a moored instrument. J Atmos Ocean Technol. 31(2):474–490.

Ferreira RM, Estefen SF, Romeiser R. 2016. Under what conditions SAR along-track interferometry is suitable for assessment of tidal energy resource. IEEE J Selec Top Appl Earth Observ Remote Sens. 9(11):5011–5022.

Froude LSR, Bengtsson L, Hodges KI. 2013. Atmospheric predictability revisited. Tellus A Dyn Meteorol Oceanogr. 65 (1):19022.

Gaspar P, Benson S, Dutton P, Réveillère A, Jacob G, Meetoo C, Dehecq A, Fossette S. 2012. Oceanic dispersal of juvenile leatherback turtles: going beyond passive drift modeling. Mar Ecol Prog Ser. 457:265–284.

Gemmrich J, Garrett C. 2012. The signature of inertial and tidal currents in offshore wave records. J Phys Oceanogr. 42(6):1051–1056.

Gentemann CL. 2003. Diurnal signals in satellite sea surface temperature measurements. Geophys Res Lett. 30 (3):1140.

Giarrusso C, Carratelli EP, Spulsi G. 2001. On the effects of wave drift on the dispersion of floating pollutants. Ocean Eng. 28(10):1339–1348.

Gillibrand PA, Willis KJ. 2007. Dispersal of sea louse larvae from salmon farms: modelling the influence of environmental conditions and larval behaviour. Aquatic Biol. 1 (1):63–75.

Gneiting T, Raftery AE. 2005. Weather forecasting with ensemble methods. Science. 310(5746):248–249.

Goldstein RM, Zebker HA. 1987. Interferometric radar measurement of ocean surface currents. Nature. 328 (6132):707–709.

Gonella J. 1972. A rotary-component method for analysing meteorological and oceanographic vector time series. Deep Sea Res. 19:833–846.

Gopalakrishnan G, Blumberg AF. 2012. Assimilation of HF radar-derived surface currents on tidal-timescales. J Oper Oceanogr. 5(1):75–87.

Gough MK, Beron-Vera FJ, Olascoaga MJ, Sheinbaum J, Jouanno J, Duran R. 2019. Persistent lagrangian transport patterns in the Northwestern Gulf of Mexico. J Phys Oceanogr. 49(2):353–367.

Griffa A, Kirwan J, D. A, Mariano AJ, Özgökmen T, Rossby HT, editor. 2007. Lagrangian analysis and prediction of coastal and ocean dynamics. Cambridge: Cambridge University Press.

Griffies SM. 2004. Fundamentals of ocean climate models. Princeton and Oxford: Princeton University Press.

Grotmaack R, Meylan MH. 2006. Wave forcing of small floating bodies. J Waterway Port Coastal Ocean Eng. 132(3):192–198.

Gurgel KW, Antonischki G, Essen HH, Schlick T. 1999. Wellen radar (WERA): a new ground-wave HF radar for ocean remote sensing. Coast Eng. 37(3):219–234.

Haelters J, Jauniaux T, Kerckhof F, Ozer J, Scory S. 2006. Using models to investigate a harbour porpoise bycatch problem in the southern North Sea–eastern Channel in spring 2005. ICES CM. 50:3–12.

Hansen MW, Johannessen JA, Dagestad KF, Collard F, Chapron B. 2011. Monitoring the surface inflow of Atlantic Water to the Norwegian Sea using Envisat ASAR. J Geophys Res Oceans. 116(C12):C12008.

Harrington-Missin L, Calverley M, Jeans G. 2009. Synergistic use of satellite and in-situ current data to improve the characterisation of seasonal trends. In: Proceeding of the 28th ASME; Honolulu, USA. p. 667–671.

Heron M, Gomez R, Weber B, Dzvonkovskaya A, Helzel T, Thomas N, Wyatt L. 2016. Application of HF Radar in Hazard Management.

Houghton D. 1969. Acapulco'68. Weather. 24(1):2–18.

Houghton D, Woods J. 1969. The slippery seas of acapulco. New Sci. 16:134–136.

Hrycik JM, Chassé J, Ruddick BR, Taggart CT. 2013. Dispersal kernel estimation: a comparison of empirical and modelled particle dispersion in a coastal marine system. Estuar Coast Shelf Sci. 133:11–22.

Huang G, Law AW-K, Huang Z. 2011. Wave-induced drift of small floating objects in regular waves. Ocean Eng. 38 (4):712–718.

Huang W, Wu X, Lund B, El-Darymli K. 2017. Advances in coastal HF and microwave (S- or X-band) radars.

Isern-Fontanet J, Ballabrera-Poy J, Turiel A, García-Ladona E. 2017. Remote sensing of ocean surface currents: a review of what is being observed and what is being assimilated. Nonlinear Process Geophys. 24(4):613–643.

Jacobs GA, Bartels BP, Bogucki DJ, Beron-Vera FJ, Chen SS, Coelho EF, Curcic M, Griffa A, Gough M, Haus BK, et al. 2014a. Data assimilation considerations for improved ocean predictability during the Gulf of Mexico Grand Lagrangian Deployment (GLAD). Ocean Model. 83:98–117.

Jacobs GA, Richman JG, Doyle JD, Spence PL, Bartels BP, Barron CN, Helber RW, Bub FL. 2014b. Simulating conditional deterministic predictability within ocean frontogenesis. Ocean Model. 78:1–16.

Janeković I, Powell BS, Matthews D, McManus MA, Sevadjian J. 2013. 4D-Var data assimilation in a nested, coastal ocean model: a hawaiian case study. J Geophys Res Oceans. 118 (10):5022–5035.

Janssen P. 2012. Ocean wave effects on the daily cycle in SST. J Geophys Res. 117(null):C00J32.

Jeans G, Fox J, Channelliere C. 2014. Current profile data sources for engineering design West of Shetlands. In: Proceedings of the 33rd AMSE; San Francisco (CA). p. V08BT06A036.

Jeans G, Lefevre F. 2008. Evolving synergies in applied ocean current measurement. J Oper Oceanogr. 1(1):45–49.

Jenkins AD. 1989. The use of a wave prediction model for driving a near-surface current model. D Hydrogr Z. 42:133–149.

Johannessen JA, Chapron B, Collard F, Kudryavtsev V, Mouche A, Akimov D, Dagestad K-F. 2008. Direct ocean surface velocity measurements from space: improved quantitative interpretation of Envisat ASAR observations. Geophys Res Lett. 35(22):L22608.

Johannessen JA, Chapron B, Collard F, Rio MH, Piollé JF, Gaultier L, Quartly G, Shutler J, Escola R, Raj R, et al.

2016. GlobCurrent : Multisensor synergy for surface current estimation. In: Proceedings of Living Planet Symposium 2016. Prague, Czech Republic: ESA.

Jones CE, Dagestad K-F, Breivik O, Holt B, Röhrs J, Christensen KH, Espeseth M, Brekke C, Skrunes S. 2016. Measurement and modeling of oil slick transport. J Geophys Res Oceans. 121:7759–7775.

Kawai Y, Wada A. 2007. Diurnal sea surface temperature variation and its impact on the atmosphere and ocean: a review. J Oceanogr. 63(5):721–744.

Keghouche I, Bertino L, Lisæter KA. 2009. Parameterization of an iceberg drift model in the Barents Sea. J Atmos Ocean Technol. 26(10):2216–2227.

Komen GJ, Cavaleri L, Doneland M, Hasselmann K, Hasselmann S, Janssen PAE. 1994. Dynamics and modelling of ocean waves. Cambridge: Cambridge University Press.

Koszalka I, LaCasce JH, Orvik KA. 2009. Relative dispersion in the Nordic Seas. J Mar Res. 67:411–433.

Kudryavtsev VN, Soloviev AV. 1990. Slippery near-surface layer of the ocean arising due to daytime solar heating. J Phys Oceanogr. 20(5):617–628.

Kukulka T, Proskurowski G, Morét-Ferguson S, Meyer DW, Law KL. 2012. The effect of wind mixing on the vertical distribution of buoyant plastic debris. Geophys Res Lett. 39(7):L07601.

Lacasce JH. 2000. Floats and f/H. J Mar Res. 58(1):61–95.

LaCasce JH. 2008. Statistics from Lagrangian observations. Prog Oceanogr. 77:1–29.

LaCasce JH. 2017. The prevalence of oceanic surface modes. Geophys Res Lett. 44(21):11097–11105.

LaCasce JH, Bower A. 2000. Relative dispersion in the subsurface North Atlantic. J Mar Res. 58:863–894.

LaCasce JH, Mahadevan A. 2006. Estimating subsurface horizontal and vertical velocities from sea-surface temperature. J Mar Res. 64(5):695–721.

LaCasce JH, Ohlmann C. 2003. Relative dispersion at the surface of the Gulf of Mexico. J Mar Res. 61(3):285–312.

LaCasce JH, Wang J. 2015. Estimating subsurface velocities from surface fields with idealized stratification. J Phys Oceanogr. 45(9):2424–2435.

Lange P, Hühnerfuss H. 1978. Drift response of monomolecular slicks to wave and wind action. J Phys Oceanogr. 8(1):142–150.

Langmuir I. 1938. Surface motion of water induced by wind. Science. 87:119–123.

Lapeyre G, Klein P. 2006. Dynamics of the upper oceanic layers in terms of surface quasigeostrophy theory. J Phys Oceanogr. 36(2):165–176.

Large WG, McWilliams JC, Doney S. 1994. Oceanic vertical mixing: a review and a model with a nonlocal boundary layer parameterization. Rev Geophys. 32:363–403.

Lavergne T. 2009. Validation and monitoring of the OSI SAF low resolution sea ice drift product. High Latitude center of the Ocean & Sea Ice Satellite Application Facility. Technical Report.

Law KL. 2017. Plastics in the marine environment. Ann Rev Mar Sci. 9:205–229.

Laxague NJM, Haus BK, Ortiz-Suslow DG, Smith CJ, Novelli G, Dai H, Özgökmen T, Graber HC. 2017. Passive optical sensing of the near-surface wind-driven current profile. J Atmos Ocean Technol. 34(5):1097–1111.

Laxague NJM, Özgökmen TM, Haus BK, Novelli G, Shcherbina A, Sutherland P, Guigand CM, Lund B,

Mehta S, Alday M, et al. 2018. Observations of near surface current shear help describe oceanic oil and plastic transport. Geophys Res Lett. 45(1):245–249.

Lenn Y-D, Chereskin TK. 2009. Observations of Ekman currents in the southern ocean. J Phys Oceanogr. 39(3):768–779.

Lentz SJ. 2001. The influence of stratification on the wind-driven cross-shelf circulation over the North Carolina shelf. J Phys Oceanogr. 31(9):2749–2760.

Le Traon P-Y, Antoine D, Bentamy A, Bonekamp H, Breivik LA, Chapron B, Corlett G, Dibarboure G, DiGiacomo P, Donlon C, et al. 2015. Use of satellite observations for operational oceanography: recent achievements and future prospects. J Oper Oceanogr. 8(sup1):s12–s27.

Lewis D, Belcher S. 2004. Time-dependent, coupled, Ekman boundary layer solutions incorporating Stokes drift. Dynam Atmos Oceans. 37(4):313–351.

Lewis HW, Sanchez JMC, Siddorn J, King RR, Tonani M, Saulter A, Sykes P, Pequignet A-C, Weedon GP, Palmer T, et al. 2019. Can wave coupling improve operational regional ocean forecasts for the north-west European Shelf? Ocean Sci. 15(3):669–690.

Lilly JM, Gascard J-C. 2006. Wavelet ridge diagnosis of time-varying elliptical signals with application to an oceanic eddy. Nonlinear Process Geophys. 13(5):467–483.

Longuet-Higgins MS. 1953. Mass transport in water waves. Philos Trans R Soc London Ser A. 245:535–581.

Lorenz EN. 1969. The predictability of a flow which possesses many scales of motion. Tellus. 21(3):289–307.

Lorenz EN. 1982. Atmospheric predictability experiments with a large numerical model. Tellus. 34(6):505–513.

Lucas DM, Etienne DH, Greiner DE, CLS DMB. 2012. A new approach to surface currents monitoring. J Oper Oceanogr. 5(2):3–10.

Lumpkin R, Özgökmen T, Centurioni L. 2017. Advances in the application of surface drifters. Ann Rev Mar Sci. 9(1):59–81.

Madsen OS. 1977. A realistic model of the wind-induced Ekman boundary layer. J Phys Oceanogr. 7(2):248–255.

Mariano AJ, Ryan EH, Huntley HS, Laurindo L, Coelho E, Griffa A, Özgökmen TM, Berta M, Bogucki D, Chen SS, et al. 2016. Statistical properties of the surface velocity field in the northern Gulf of Mexico sampled by GLAD drifters. J Geophys Res Oceans. 121(7):5193–5216.

Marsh JG, Martin TV. 1982. The SEASAT altimeter mean sea surface model. J Geophys Res Oceans. 87(C5):3269–3280.

Matthews JP, Ostrovsky L, Yoshikawa Y, Komori S, Tamura H. 2017. Dynamics and early post-tsunami evolution of floating marine debris near Fukushima Daiichi. Nat Geosci. 10(8):598–603.

McCann DL, Bell PS. 2014. Marine radar derived current vector mapping at a planned commercial tidal stream turbine array in the Pentland Firth, U.K. In: 2014 Oceans – St. John's. p. 1–4.

McGovern DJ, Bai W. 2014. Experimental study on kinematics of sea ice floes in regular waves. Cold Reg Sci Technol. 103:15–30.

McWilliams JC. 2016. Submesoscale currents in the ocean. Proc R Soc A Math Phys Eng Sci. 472(2189):20160117.

McWilliams JC, Huckle E, Liang J-H, Sullivan PP. 2012. The wavy Ekman Layer: Langmuir circulations, breaking waves, and Reynolds stress. J Phys Oceanogr. 42:1793–1816.

Mellor G. 2005. Some consequences of the three-dimensional current and surface wave equations. J Phys Oceanogr. 35 (11):2291–2298.

Monismith SG, Fong DA. 2004. A note on the potential transport of scalars and organisms by surface waves. Limnol Oceanogr. 49:1214–1217.

Moore AM, Arango HG, Broquet G, Powell BS, Weaver AT, Zavala-Garay J. 2011. The regional ocean modeling system (ROMS) 4-dimensional variational data assimilation systems: part I – system overview and formulation. Prog Oceanogr. 91(1):34–49.

Morey SL, Wienders N, Dukhovskoy DS, Bourassa MA. 2018. Measurement characteristics of near-surface currents from ultra-thin drifters, drogued drifters, and HF radar. Remote Sens. 10(10):1633.

Mouche AA, Collard F, Chapron B, Dagestad K, Guitton G, Johannessen JA, Kerbaol V, Hansen MW. 2012. On the use of doppler shift for sea surface wind retrieval from SAR. IEEE Trans Geosci Remote Sens. 50(7):2901–2909.

Niiler PP, Paduan JD. 1995. Wind-driven motions in the Northeast Pacific as measured by Lagrangian drifters. J Phys Oceanogr. 25:2819–2830.

Nonaka M, Sasai Y, Sasaki H, Taguchi B, Nakamura H. 2016. How potentially predictable are midlatitude ocean currents? Sci Rep. 6:20153.

Novelli G, Guigand CM, Cousin C, Ryan EH, Laxague NJM, Dai H, Haus BK, Özgökmen TM. 2017. A biodegradable surface drifter for ocean sampling on a massive scale. J Atmos Ocean Technol. 34(11):2509–2532.

O'Brien JJ. 1970. A note on the vertical structure of the Eddy exchange coefficient in the planetary boundary layer. J Atmos Sci. 27(8):1213–1215.

Ohlmann C, White P, Washburn L, Terrill E, Emery B, Otero M. 2007. Interpretation of coastal HF radar-derived surface currents with high-resolution drifter data. J Atmos Ocean Tech. 24:666–680.

Oke PR, Larnicol G, Fujii Y, Smith GC, Lea DJ, Guinehut S, Remy E, Balmaseda MA, Rykova T, Surcel-Colan D, et al. 2015a. Assessing the impact of observations on ocean forecasts and reanalyses: part 1, global studies. J Oper Oceanogr. 8(sup1):s49–s62.

Oke PR, Larnicol G, Jones EM, Kourafalou V, Sperrevik AK, Carse F, Tanajura CAS, Mourre B, Tonani M, Brassington GB, et al. 2015b. Assessing the impact of observations on ocean forecasts and reanalyses: part 2, regional applications. J Oper Oceanogr. 8(sup1):s63–s79.

Oke PR, Sakov P, Cahill ML, Dunn JR, Fiedler R, Griffin DA, Mansbridge JV, Ridgway KR, Schiller A. 2013. Towards a dynamically balanced eddy-resolving ocean reanalysis: Bran3. Ocean Model. 67:52–70.

Okubo A. 1971. Oceanic diffusion diagrams. Deep Sea Res Oceanogr Abstr. 18(8):789–802.

Pascual A, Faugère Y, Larnicol G, Traon P-YL. 2006. Improved description of the ocean mesoscale variability by combining four satellite altimeters. Geophys Res Lett. 33(2).

Pasmans I, Kurapov AL. 2019. Ensemble of 4DVARs (En4DVar) data assimilation in a coastal ocean circulation model, part I: methodology and ensemble statistics. Ocean Model. 144:101493.

Pawlowicz R, Beardsley B, Lentz S. 2002. Classical tidal harmonic analysis including error estimates in MATLAB using T_tide. Comput Geosci. 28(8):929–937.

Pedlosky J. 1987. Geophysical fluid dynamics. New York: Springer Science & Business Media.

Peltier H, Dabin W, Daniel P, Van Canneyt O, Dorémus G, Huon M, Ridoux V. 2012. The significance of stranding data as indicators of cetacean populations at sea: modelling the drift of cetacean carcasses. Ecol Indic. 18:278–290.

Penduff T, Juza M, Barnier B, Zika J, Dewar WK, Treguier A-M, Molines J-M, Audiffren N. 2011. Sea level expression of intrinsic and forced ocean variabilities at interannual time scales. J Clim. 24(21):5652–5670.

Perrie W, Tang CL, Hu Y, DeTracy BM. 2003. The impact of waves on surface currents. J Phys Oceanogr. 33(10):2126–2140.

Phillips OM. 1977. The dynamics of the upper ocean. London: Cambridge University Press.

Phillipson L, Toumi R. 2017. Impact of data assimilation on ocean current forecasts in the Angola Basin. Ocean Model. 114:45–58.

Pollard RT, Millard RC. 1970. Comparison between observed and simulated wind-generated inertial oscillations. Deep Sea Res Oceanogr Abstr. 17(4):813–821.

Polton JA, Lewis DM, Belcher SE. 2005. The role of wave-induced Coriolis-Stokes forcing on the wind-driven mixed layer. J Phys Oceanogr. 35(4):444–457.

Potemra JT. 2012. Numerical modeling with application to tracking marine debris. Mar Pollut Bull. 65:42–50.

Poulain P-M, Gerin R, Mauri E, Pennel R. 2009. Wind effects on drogued and undrogued drifters in the eastern mediterranean. J Atmos Ocean Technol. 26:1144–1156.

Poulain P-M, Luther DS, Patzert WC. 1992. Deriving inertial wave characteristics from surface drifter velocities: frequency variability in the tropical Pacific. J Geophys Res Oceans. 97(C11):17947–17959.

Powell B, Arango H, Moore A, Lorenzo ED, Milliff R, Foley D. 2008. 4dvar data assimilation in the intra-americas sea with the regional ocean modeling system (roms). Ocean Model. 23(3):130–145.

Price JF, Weller RA, Pinkel R. 1986. Diurnal cycling: Observations and models of the upper ocean response to diurnal heating, cooling, and wind mixing. J Geophys Res Oceans. 91(C7):8411–8427.

Ralph EA, Niiler PP. 1999. Wind-driven currents in the tropical Pacific. J Phys Oceanogr. 29(9):2121–2129.

Restrepo J, Ramírez J, Venkataramani S, Restrepo JM, Ramírez JM, Venkataramani S. 2015. An oil fate model for shallow-waters. J Mar Sci Eng. 3(4):1504–1543.

Richardson LF. 1926. Atmospheric diffusion shown on a distance-neighbour graph. Proc R Soc London Ser A. 110 (756):709–737. Containing Papers of a Mathematical and Physical Character.

Richardson LF, Stommel H. 1948. Note on eddy diffusion in the sea. J Meteorol. 5:238–240.

Rio M-H, Hernandez F. 2003. High-frequency response of wind-driven currents measured by drifting buoys and altimetry over the world ocean. J Geophys Res. 108(C8):3283.

Rio M-H, Mulet S, Picot N. 2014. Beyond GOCE for the ocean circulation estimate: synergetic use of altimetry, gravimetry, and in situ data provides new insight into geostrophic and Ekman currents. Geophys Res Lett. 41 (24):8918–8925.

Rixen M, Book JW, Carta A, Grandi V, Gualdesi L, Stoner R, Ranelli P, Cavanna A, Zanasca P, Baldasserini G, et al. 2009.

Improved ocean prediction skill and reduced uncertainty in the coastal region from multi-model super-ensembles. J Mar Syst. 78:S282–S289.

Røed LP. 1977. A note on time-dependent Ekman theory. Dynam Atmos Oceans. 1(3):273–276.

Røed LP. 2018. Atmospheres and oceans on computers – fundamental numerical methods for geophysical fluid dynamics. Springer. https://www.springer.com/gp/book/9783319938639

Röhrs J, Christensen KH. 2015. Drift in the uppermost part of the ocean. Geophy Res Lett. 42:1–8.

Röhrs J, Christensen KH, Hole LR, Broström G, Drivdal M, Sundby S. 2012. Observation-based evaluation of surface wave effects on currents and trajectory forecasts. Ocean Dynam. 62:1519–1533.

Röhrs J, Christensen KH, Vikebø FB, Sundby S, Saetra O, Broström G. 2014. Wave-induced transport and vertical mixing of pelagic eggs and larvae. Limnol Oceanogr. 59 (4):1213–1227.

Röhrs J, Dagestad K-F, Asbjørnsen H, Nordam T, Skancke J, Jones CE, Brekke C. 2018a. The effect of vertical mixing on the horizontal drift of oil spills. Ocean Sci. 14(6):1581–1601.

Röhrs J, Sperrevik AK, Christensen KH. 2018b. NorShelf: An ocean reanalysis and data-assimilative forecast model for the Norwegian shelf sea. Oslo, Norway: Norwegian Meteorological Institute. Technical Report ISSN 2387-4201 04/2018.

Röhrs J, Sperrevik AK, Christensen KHA, Broström G, Breivik O. 2015. Comparison of HF radar measurements with Eulerian and Lagrangian surface currents. Ocean Dynam. 65(5):679–690.

Romeiser R. 2013. The future of SAR-based oceanography: high-resolution current measurements by along-track interferometry. Oceanography. 26(2).

Romeiser R, Breit H, Eineder M, Runge H, Flament P, Jong K d., Vogelzang J. 2005. Current measurements by SAR along-track interferometry from a Space Shuttle. IEEE Trans Geosci Remote Sens. 43(10):2315–2324.

Romeiser R, Runge H, Suchandt S, Kahle R, Rossi C, Bell PS. 2014. Quality assessment of surface current fields from TerraSAR-X and TanDEM-X along-track interferometry and doppler centroid analysis. IEEE Trans Geosci Remote Sens. 52(5):2759–2772.

Romeiser R, Suchandt S, Runge H, Steinbrecher U, Grunler S. 2010. First analysis of TerraSAR-X along-track InSAR-derived current fields. IEEE Trans Geosci Remote Sens. 48(2):820–829.

Rouault MJ, Mouche A, Collard F, Johannessen JA, Chapron B. 2010. Mapping the Agulhas current from space: an assessment of ASAR surface current velocities. J Geophys Res Oceans. 115(C10):C10026.

Rubio A, Mader J, Corgnati L, Mantovani C, Griffa A, Novellino A, Quentin C, Wyatt L, Schulz-Stellenfleth J, Horstmann J, et al. 2017. HF radar activity in European coastal seas: next steps toward a Pan-European HF radar network. Front Mar Sci. 4:8.

Rypina II, Kirincich AR, Limeburner R, Udovydchenkov IA. 2014. Eulerian and lagrangian correspondence of high-frequency radar and surface drifter data: effects of radar resolution and flow components. J Atmos Ocean Technol. 31(4):945–966.

Saetra O, Albretsen J, M. Janssen PAE. 2007. Sea-state-dependent momentum fluxes for ocean modeling. J Phys Oceanogr. 37(11):2714–2725.

Sakov P, Counillon F, Bertino L, Lisæter KA, Oke PR, Korablev A. 2012. TOPAZ4: an ocean-sea ice data assimilation system for the North Atlantic and Arctic. Ocean Sci. 8 (4):633–656.

Sandery PA, Sakov P. 2017. Ocean forecasting of mesoscale features can deteriorate by increasing model resolution towards the submesoscale. Nat Commun. 8(1):1566.

Saunders PM. 1976. Near-surface current measurements. Deep Sea Res Oceanogr Abstr. 23(3):249–257.

Sebastiõ P, Soares CG. 2006. Uncertainty in predictions of oil spill trajectories in a coastal zone. J Mar Syst. 63 (3-4):257–269.

Sentchev A, Forget P, Fraunié P. 2017. Surface current dynamics under sea breeze conditions observed by simultaneous HF radar, ADCP and drifter measurements. Ocean Dyn. 67(3-4):499–512.

Shay L, Cook T, Peters H, Mariano A, Weisberg R, An P, Soloviev A, Luther M. 2002. Very high-frequency radar mapping of surface currents. IEEE J Ocean Eng. 27 (2):155–169.

Shen HH, Zhong Y. 2001 Dec. Theoretical study of drift of small rigid floating objects in wave fields. J Waterway Port Coast Ocean Eng. 127:343–351.

Shrira VI, Forget P. 2015. On the nature of near-inertial oscillations in the uppermost part of the ocean and a possible route toward HF radar probing of stratification. J Phys Oceanogr. 45(10):2660–2678.

Shrira VI, Ivonin DV, Broche P, de Maistre JC. 2001. On remote sensing of vertical shear of ocean surface currents by means of a single-frequency VHF radar. Geophys Res Lett. 28(20):3955–3958.

Shutler JD, Quartly GD, Donlon CJ, Sathyendranath S, Platt T, Chapron B, Johannessen JA, Girard-Ardhuin F, Nightingale PD, Woolf DK, et al. 2016. Progress in satellite remote sensing for studying physical processes at the ocean surface and its borders with the atmosphere and sea ice. Prog Phys Geogr. 40(2):215–246.

Simecek-Beatty D, Lehr WJ. 2017. Extended oil spill spreading with Langmuir circulation. Mar Pollut Bull. 122(1):226–235.

Smith SD. 1993. Hindcasting iceberg drift using current profiles and winds. Cold Reg Sci Technol. 22:33–45.

Sobey RJ, Barker CH, Spring F. 1997. Wave-driven transport of surface oil. J Coast Res. 13(2):490–496.

Sperrevik AK, Christensen KH, Röhrs J. 2015. Constraining energetic slope currents through assimilation of high-frequency radar observations. Ocean Sci. 11:237–249.

Sperrevik AK, Röhrs J, Christensen KH. 2017. Impact of data assimilation on Eulerian versus Lagrangian estimates of upper ocean transport. J Geophys Res Oceans. 122 (7):5445–5457.

Stammer D, Griffies SM. 2017. Ocean modeling and data assimilation in the context of satellite altimetry. In: Satellite altimetry over oceans and land surfaces. Taylor and Francies. p. 34.

Staneva J, Alari V, Breivik O, Bidlot J-R, Mogensen K. 2017. Effects of wave-induced forcing on a circulation model of the North Sea. Ocean Dyn. 67:81–101.

Stewart RH, Joy JW. 1974. HF radio measurements of surface currents. Deep Sea Res. 21:1039–1049.

Stokes GG. 1847. On the theory of oscillatory waves. Trans Camb Phil Soc. 8:441–473.

Stuart-Menteth AC. 2003. A global study of diurnal warming using satellite-derived sea surface temperature. J Geophys Res. 108(C5):3155.

Stull RB. 1988. An introduction to boundary layer meteorology. Dordrecht: Kluwer Academic Publishers.

Sutherland G, Marié L, Reverdin G, Christensen KH, Broström G, Ward B. 2016. Enhanced turbulence associated with the diurnal jet in the ocean surface boundary layer. J Phys Oceanogr. 46(10):3051–3067.

Talley L, Pickard G, Emergy W, Swift J. 2011. Descriptive physical oceanography: an introduction. Academic Press, Elsevier science. https://www.sciencedirect.com/book/9780750645522/descriptive-physical-oceanography?via=ihub=

Tandeo P, Atencia A, Haro CG. 2016. Combining 15 years of microwave SST and along-track SSH to estimate ocean surface currents. In: 6th International Workshop on Climate Informatics; Boulder, Co, USA.

Tang C, Perrie W, Jenkins A, DeTracey B, Hu Y, Toulany B, Smith P. 2007. Observation and modeling of surface currents on the Grand Banks: A study of the wave effects on surface currents. J Geophys Res. 112(C10):C10025.

Teague C, Vesecky J, Hallock Z. 2001. A comparison of multi-frequency HF radar and ADCP measurements of near-surface currents during COPE-3. IEEE J Ocean Eng. 26(3):399–405.

Thomas LN, Tandon A, Mahadevan A. 2008. Submesoscale processes and dynamics. Geophys Monogr Ser. 177:17–38. Washington DC American Geophysical Union.

Tonani M, Balmaseda M, Bertino L, Blockley E, Brassington G, Davidson F, Drillet Y, Hogan P, Kuragano T, Lee T, et al. 2015. Status and future of global and regional ocean prediction systems. J Oper Oceanogr. 8(sup2):s201–s220.

Toporkov JV, Perkovic D, Farquharson G, Sletten MA, Frasier SJ. 2005. Sea surface velocity vector retrieval using dual-beam interferometry: first demonstration. IEEE Trans Geosci Remote Sens. 43(11):2494–2502.

Trinanes JA, Olascoaga MJ, Goni GJ, Maximenko NA, Griffin DA, Hafner J. 2016. Analysis of flight MH370 potential debris trajectories using ocean observations and numerical model results. J Oper Oceanogr. 9(2):126–138.

Uchiyama Y, McWilliams J, Shchepetkin A. 2010. Wave-current interaction in an oceanic circulation model with a vortex-force formalism: application to the surf zone. Ocean Model. 34:16–35.

Umlauf L, Burchard H. 2005. Second-order turbulence closure models for geophysical boundary layers. A review of recent work. Cont Shelf Res. 25(7–8):795–827.

Vallis G. 2017. Atmospheric and oceanic fluid dynamics. Cambridge: Cambridge University Press.

van den Bremer TS, Breivik O. 2018. Stokes drift. Philos Trans R Soc A Math Phys Eng Sci. 376(2111). DOI:10.1098/rsta.2017.0104

van Sebille E, Griffies SM, Abernathey R, Adams TP, Berloff P, Biastoch A, Blanke B, Chassignet EP, Cheng Y, Cotter CJ, et al. 2018. Lagrangian ocean analysis: fundamentals and practices. Ocean Model. 121:49–75.

Vialard J, Vitart F, Balmaseda MA, Stockdale TN, Anderson DLT. 2005. An ensemble generation method for seasonal forecasting with an ocean–atmosphere coupled model. Mon Weather Rev. 133(2):441–453.

Vikebø FB, Ådlandsvik B, Albretsen J, Sundby S, Stenevik EKR, Huse G, Svendsen E, Kristiansen T, Eriksen E. 2011. Real-time ichthyoplankton drift in northeast arctic cod and norwegian spring-spawning herring. PLoS ONE. 6(11):e27367.

Wang J, Flierl GR, LaCasce JH, McClean JL, Mahadevan A. 2013. Reconstructing the ocean's interior from surface data. J Phys Oceanogr. 43(8):1611–1626.

Warner JC, Sherwood CR, Arango HG, Signell RP. 2005. Performance of four turbulence closure models implemented using a generic length scale method. Ocean Model. 8(1–2):81–113.

Warner JC, Sherwood CR, Signell R, Harris C, Arango H. 2008. Development of a three-dimensional, regional, coupled wave, current, and sediment-transport model. Comput Geosci. 34(10):1284–1306.

Warren MA, Quartly GD, Shutler JD, Miller PI, Yoshikawa Y. 2016. Estimation of ocean surface currents from maximum cross correlation applied to GOCI geostationary satellite remote sensing data over the Tsushima (Korea) Straits. J Geophys Res Oceans. 121(9):6993–7009.

Weber J, Broström G, Saetra Ø. 2006. Eulerian vs Lagrangian approaches to the wave-induced transport in the upper ocean. J Phys Oceanogr. 36:2106–2118.

Wichmann D, Delandmeter P, van Sebille E. 2019. Influence of near-surface currents on the global dispersal of marine microplastic. J Geophys Res Oceans. 124(8):6086–6096.

Williamson D, Goldstein M, Allison L, Blaker A, Challenor P, Jackson L, Yamazaki K. 2013. History matching for exploring and reducing climate model parameter space using observations and a large perturbed physics ensemble. Clim Dyn. 41(7):1703–1729.

Wu J. 1984. Viscous sublayer below a wind-disturbed water surface. J Phys Oceanogr. 14(1):138–144.

Xie J, Bertino L, Counillon F, Lisæter KA, Sakov P. 2017. Quality assessment of the TOPAZ4 reanalysis in the Arctic over the period 1991–2013. Ocean Sci. 13(1):123–144.

Xu Z, Bowen AJ. 1994. Wave- and wind-driven flow in water of finite depth. J Phys Oceanogr. 24:1850.

Xue Y, Wen C, Kumar A, Balmaseda M, Fujii Y, Alves O, Martin M, Yang X, Vernieres G, Desportes C, et al. 2017. A real-time ocean reanalyses intercomparison project in the context of tropical pacific observing system and ENSO monitoring. Clim Dyn. 49(11):3647–3672.

Zhang H. 2017. Transport of microplastics in coastal seas. Estuar Coast Shelf Sci. 199:74–86.

Zhang H-M, Prater MD, Rossby T. 2001. Isopycnal Lagrangian statistics from the North Atlantic Current RAFOS float observations. J Geophys Res Oceans. 106(C7):13817–13836.

Zuo H, Balmaseda MA, Mogensen K. 2017. The new eddy-permitting orap5 ocean reanalysis: description, evaluation and uncertainties in climate signals. Clim Dyn. 49(3):791–811.